NASA TECHNICAL REPORT

NASA TR R-247

NASA TR R-247

A SYSTEM FOR INERTIAL EXPERIMENT POINTING AND ATTITUDE CONTROL

by Peter R. Kurzhals and Carolyn Grantham

Langley Research Center

Langley Station, Hampton, Va.

NATIONAL AERONAUTICS AND SPACE ADMINISTRATION • WASHINGTON, D. C. • AUGUST 1966

NASA TR R-247

A SYSTEM FOR INERTIAL EXPERIMENT POINTING AND ATTITUDE CONTROL

By Peter R. Kurzhals and Carolyn Grantham

Langley Research Center
Langley Station, Hampton, Va.

NATIONAL AERONAUTICS AND SPACE ADMINISTRATION

For sale by the Clearinghouse for Federal Scientific and Technical Information
Springfield, Virginia 22151 – Price $2.50

A SYSTEM FOR INERTIAL EXPERIMENT POINTING AND ATTITUDE CONTROL

By Peter R. Kurzhals and Carolyn Grantham
Langley Research Center

SUMMARY

A system for inertial experiment pointing and attitude control (designated SIXPAC) of future manned spacecraft has been investigated. The SIXPAC concept consists of three double-gimbaled control moment gyros alined with the axes of the spacecraft, and derives its control torques from precession of the gyro wheels. This system is readily mechanized, has inherent redundancy, and should provide a wider range of attitude control for manned spacecraft than the gyro systems previously considered. The SIXPAC can provide both the large range of control torques and the fine attitude holds associated with spacecraft experiments such as earth-surface tracking and mapping, photographic missions, and astronomical observations. Periodic aerodynamic and gravity-gradient torques can also be counteracted by the proposed system. Redundancies inherent to the three-gyro arrangement further allow reduced spacecraft control in case of failure or shutdown of one of the three gyros.

The complete equations of motion for a spacecraft with the SIXPAC were developed, and were integrated numerically on a digital computer for an example mission with a possible Apollo applications concept. Results of this computer study were used to evaluate the spacecraft and control system response and to determine the power and fuel consumption of the SIXPAC. Characteristic time histories of the attitude and angular rates of the spacecraft are presented for a number of experiments that have been proposed for typical Apollo applications missions, and the performance of the gyro system is analyzed during the control tasks associated with these experiments.

INTRODUCTION

Future manned spacecraft with extended orbital missions will house a large number of experiments, many of which will require continuous rate and attitude control of the parent spacecraft to function effectively. Earth tracking and mapping, astronomical observations, and star-tracker and sensor evaluations are examples of experiments which impose stringent control requirements on the stabilization system of the spacecraft. To perform these experiments, the spacecraft must be readily maneuverable, must be capable

of slewing rates of up to 1.2 degrees per second, and must be held to attitude and rate accuracies of 0.01 and 0.001 degree per second, respectively. (See ref. 1.) Further experiment control by gimbaling or similar means of isolation may also be necessary.

The control system for such manned spacecraft is thus faced with a formidable task. It must be capable of generating very large torques during maneuver and slewing missions, and then must produce very small control torques to obtain the attitude and rate accuracies during the actual experiment operations. While doing this, it must compensate for aerodynamic and gravity-gradient torques, crew-motion effects, and all other disturbances applied to the spacecraft.

Most of these disturbances and control tasks tend to be periodic. Aerodynamic and gravity-gradient torques are biased sinusoids, and crew-motion effects average out statistically. Maneuvers and slewing modes require cyclic control torques. Attitude and rate holds also call for small periodic control torques. When one considers that such disturbances and control tasks occur continuously throughout the orbital mission, it becomes clear that some type of momentum storage device is necessary for extended duration missions since the reaction-jet fuel required to accomplish these tasks leads to prohibitive weight penalties. (See refs. 1 and 2.)

The control moment gyroscope has been shown (refs. 1 to 6) to be the most effective means of momentum storage for long-term manned spacecraft, and the purpose of the present analysis is to consider a system for inertial experiment pointing and attitude control (designated SIXPAC) consisting of three such control moment gyros. This system is readily mechanized, has inherent redundancy, and should provide a wider range of attitude control for manned spacecraft than the gyro systems previously considered. In addition, the present three-gyro configuration with its essentially spherical momentum envelope allows lower launch weights and volumes than past systems which have used an equal or larger number of single- or double-gimbaled gyros for equivalent control tasks. (See ref. 1.) One- and two-gyro configurations are, of course, also possible and may have lower weight and volume requirements than the SIXPAC; however, the excessive complexity, undesirable cross-coupling, nonredundancy, and low reliability of such systems in general prohibit their use for manned spacecraft.

Control torques are generated by commanding the precession rate of the gyros with respect to the spacecraft, and the corresponding spacecraft and control system response are analyzed for a characteristic mission. The resultant data can be used to predict the approximate response for similar manned spacecraft and to select the control characteristics needed for such spacecraft.

SYMBOLS

e	ascent orbit eccentricity
F	external force component acting through composite mass center of spacecraft
f	torques due to mass motion within spacecraft
$\bar{G}$	control torque vector for SIXPAC
G	control torque component
$\bar{H}$	total angular momentum vector for SIXPAC
H	angular momentum of a single SIXPAC gyro
I	moment or product of inertia
I_{sp}	specific impulse
j	integer (j = 1, 2, 3, . . .)
K	constant control gain for SIXPAC gimbal rate
k	variable control gain function for SIXPAC gimbal rate
L	limiting gimbal angle ratio, $\alpha_{qpL}/90$
ℓ	desaturation jet moment arm
M	external moment component acting on spacecraft
ΔM	desaturation moment component
m	mass
n	number of moving masses within spacecraft
P	power consumption for SIXPAC
r	geocentric radius
s	Laplace transform variable
T	SIXPAC gimbal torque component
t	time

Δt	time duration of control task
W	desaturation fuel consumption
X, Y, Z	spacecraft reference axes
x,y,z	position coordinates with respect to body-fixed reference axes in the spacecraft
α	gimbal angle
η	angular position with respect to geocentric reference axes
μ	gravitational parameter of earth's central force field
ρ	approximate damping ratio for spacecraft motion with SIXPAC stabilization
τ	time constant for spacecraft motion with SIXPAC stabilization
ω_n	natural frequency for spacecraft motion with SIXPAC stabilization
φ, θ, ψ	modified Euler angles
$\overline{\Omega}$	total angular velocity vector for spacecraft
Ω	angular velocity component

Subscripts:

a	attitude
av	average value
c	commanded value
E	earth
e	experiment
F	inertially fixed coordinates
I	intermediate coordinates
i	inner gimbal
j	value of jth term where j = 1, 2, 3, . . .

L	limiting value
m	maneuver value
0	initial value
o	outer gimbal
p	component for p-axis where p = X, Y, or Z
pq,qp	SIXPAC vector component, where p and q can be x, y, or z with $p \neq q$. The first subscript denotes the SIXPAC gyro reference axis; the second subscript denotes the component reference axis. The component reference axis is a spacecraft axis for even permutations (xy,yz,zx denoted by pq) and is an intermediate gimbal axis for odd permutations (yx,xz,zy denoted by qp) of the subscripts
pj	jth value for p-axis
R	resupply or rendezvous vehicle
r	rate
S	spacecraft
s	value for composite mass center
T	slewing value
t	total value
X,Y,Z	component for the X-, Y-, or Z-axis
XY,XZ,YZ	component for the XY-, XZ-, or YZ-plane

A single prime (') denotes intermediate coordinates after first Euler rotation. A double prime (") denotes intermediate coordinates after second Euler rotation. A dot ($\dot{}$) over a symbol designates a derivative with respect to time. A bar ($\bar{}$) over a symbol designates a vector.

CONTROL SYSTEM DESCRIPTION

Configuration and Control Implementation

The SIXPAC concept, illustrated in figure 1, uses three control moment gyros to maneuver and stabilize the spacecraft. Each of these gyros consists of a flywheel spinning at a constant speed and mounted on double gimbals. These gimbals are alined with a spacecraft axis in their reference position. The outer gimbal cannot move into gimbal lock and is free to rotate continuously to take full advantage of the available momentum storage capacity. Slip rings must correspondingly be provided to pass power to the inner gimbal torquer. The inner gimbal can incur gimbal lock at $\pm 90^{\circ}$ and is limited to an angle smaller than this value by means of mechanical stops.

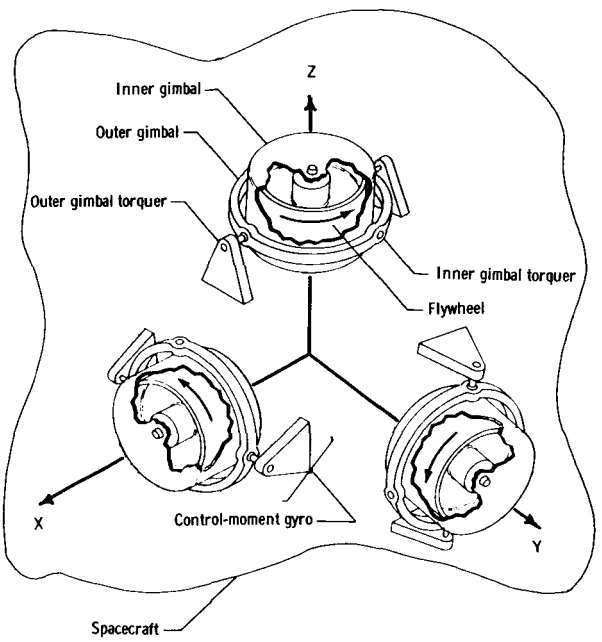

Figure 1.- Schematic of SIXPAC configuration.

Since maneuvers can best be carried out with near-spherical momentum envelopes, all the gyros are selected to have the same angular momentum. This choice of momenta may differ for spacecraft with special disturbance requirements, such as predominant torques about a particular spacecraft axis.

Control with the SIXPAC is provided by commanding the gimbal rates to be proportional to the apparent rate and attitude errors of the spacecraft. These gimbal rate commands are weighted to allow automatic transition of control to another axis and to reduce the gimbal speed as the gimbal stops are approached. Values of the control commands are developed by measuring the rates and attitude of the spacecraft, determining the deviation of these measurements from the desired rates and attitude, and then amplifying the resultant deviations by gain factors which vary with positions of the gimbal angles. The torque equations for the spacecraft and SIXPAC are given in appendix A, and the mechanization of the SIXPAC control scheme is discussed in detail in appendix B. Appendix B also presents the development of the governing equations for SIXPAC, together with a method of selecting control gains as functions of the desired damping characteristics and the spacecraft inertias.

Control Modes

Since the disturbance torques for future manned spacecraft may vary over a wide range of magnitudes and frequencies, an optimized SIXPAC should use both a coarse and a fine mode of control. During normal operation, the spacecraft may be expected to require only nominal attitude control, for example, $\pm 5^{\circ}$ with respect to its reference orientation. The SIXPAC can use a set of relatively low gains and a large time constant for this mode of control. Power consumption for large, short-duration torques (such as might arise from crew motions) will thus be minimized. For spacecraft control during experiments requiring more accurate rate and attitude holds, the SIXPAC would be switched to a fine mode of control. Crew motions will also be restricted somewhat to avoid application of large torques to the spacecraft. The SIXPAC will now use a set of high gains and a small time constant to provide the necessary accuracies. Since the disturbance torques, aside from crew motions, will be small and, in general, have low frequencies, very little power will again be required for the SIXPAC operation. Attitude accuracies of several seconds of arc and corresponding rate accuracies should be obtained during this fine control mode.

Desaturation

The presence of continuous biased periodic disturbance torques, such as may result from aerodynamic drag and gravity gradients, will saturate the SIXPAC. Provisions for desaturation must thus be made. This desaturation scheme will require a reaction-jet system capable of generating the necessary desaturation torques and driving the gimbal angles off their stops. A possible method for desaturation would apply a constant-amplitude torque pulse about a spacecraft axis when the inner gimbal angle corresponding to that axis becomes saturated while additional control torques are required. The amplitude and duration of the torque pulse are selected to reduce the associated gimbal angle magnitude by a specified percentage of its limiting value. The gimbals are automatically commanded to counteract the torque pulse and thus are desaturated. The implementation of this desaturation scheme is discussed in appendix B.

ANALYSIS AND RESULTS

Controlled Spacecraft Simulation

Coordinate definitions.- The performance of the SIXPAC was investigated by combining the control torque relations derived in appendix B with the general rotational equations of motion for a spacecraft with variable inertia characteristics. These equations of motion are given in appendix A. A numerical integration procedure for the control torque and spacecraft equations was programed on a digital computer, and the spacecraft motion was determined from the computer solutions.

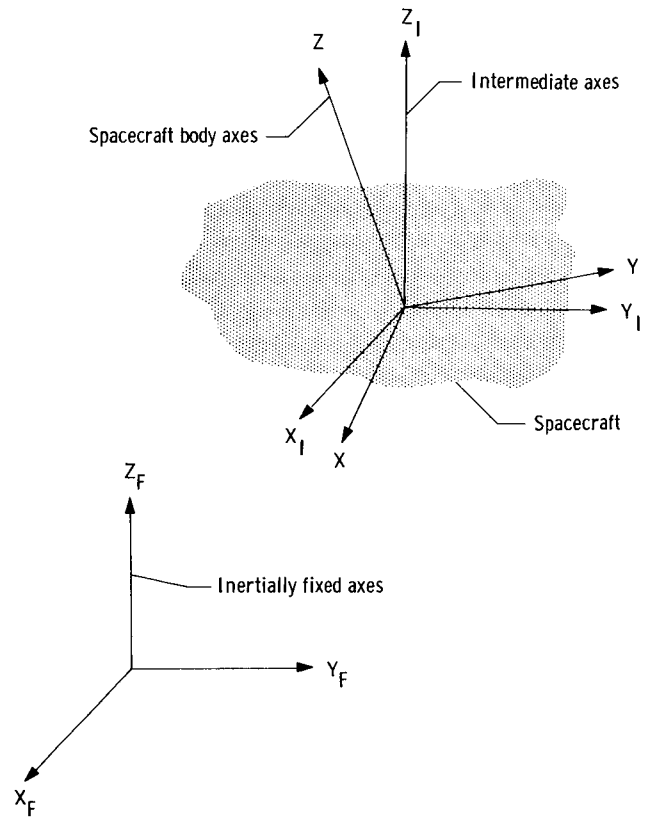

Figure 2.- Reference coordinates for spacecraft.

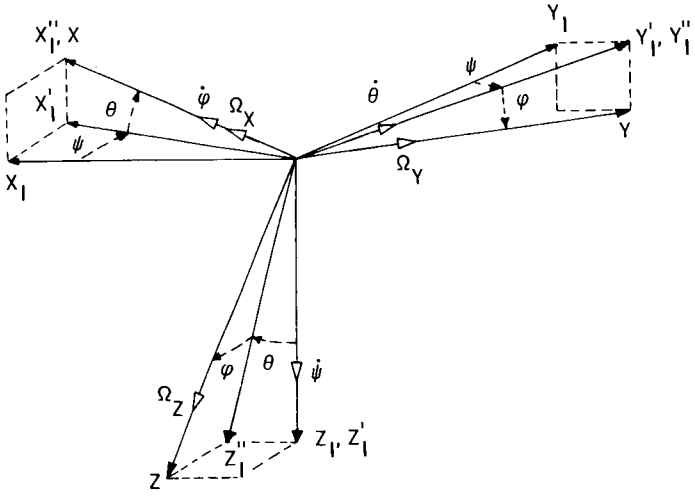

Figure 3.- Euler angle definition.

Reference coordinates for this motion are illustrated in figure 2. A set of orthogonal X, Y, and Z axes fixed to the spacecraft defines the angular motion of the spacecraft with respect to a set of intermediate orthogonal X_I, Y_I, and Z_I axes. The intermediate axes translate without rotation in inertial space, but always remain parallel to an orthogonal set of X_F, Y_F, and Z_F axes fixed in inertial space.

The inertial spacecraft attitude may thus be specified by three modified Euler angles, which determine the relative motion between the X, Y, Z and X_I, Y_I, Z_I axes. The Euler angles are designated as ψ, θ, and φ and result from three consecutive rotations about the Z_I, Y'_I, and X''_I axes. A sketch of these angles is given in figure 3.

As shown in appendix A, the Euler angles are found by relating their time derivatives to the spacecraft body rates Ω_X, Ω_Y, and Ω_Z about the X, Y, and Z axes. The body rates are then determined by numerical integration of the equations of motion of the spacecraft. Resultant values of Ω_X, Ω_Y, and Ω_Z give values for the Euler angle derivatives, and the numerical integration of the derivatives yields the Euler angles. Time histories of both the body rates and the Euler angles are used to describe the angular motion of the spacecraft.

Example mission characteristics.- A typical earth-orbital mission was chosen for the computer analysis of SIXPAC. This mission was based on an assumed Apollo

applications spacecraft shown in figure 4. Such a spacecraft could consist of an Apollo command and service module, connected to a lunar excursion module or a laboratory module. The spacecraft would be placed in a circular 200-nautical-mile (370.4-km), 28° inclination orbit by a Saturn IB booster and would have a functional lifetime of 90 to 120 days. Three astronauts would make up the crew.

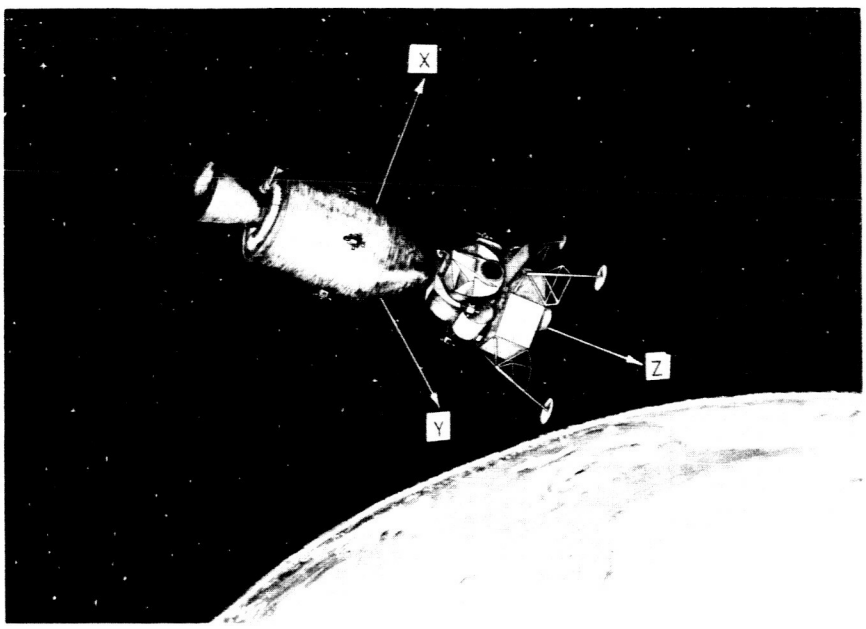

Figure 4.- Artist's concept of example spacecraft. L-66-4415

Assumed characteristics for this spacecraft are:

I_X = 151,000 slug-ft^2 = 204,729 kg-m^2

I_Y = 150,000 slug-ft^2 = 203,373 kg-m^2

I_Z = 30,000 slug-ft^2 = 40,675 kg-m^2

m_S = 600 slugs ≈ 8,760 kg

m_j = 6 slugs per astronaut ≈ 88 kg per astronaut

An example experiment program was also selected for the spacecraft. Possible control-related experiments from this program are given in table I. These experiments range from operation of a biomedical centrifuge to earth mapping and astronomical observations. Corresponding stability and control requirements, as indicated in the figure, vary from coarse attitude holds of ±5° to fine attitude pointing of 0.1 arc second. Rate requirements

similarly go from maneuver rates of $\pm 1.12^{\circ}$ per second to rate holds of $\pm 0.001^{\circ}$ per second.

TABLE I.- ASSUMED CONTROL-RELATED EXPERIMENTS FOR EXAMPLE SPACECRAFT

Experiment title	Spacecraft orientation	Required accuracies		Maximum slewing rate, deg/sec
		Attitude, deg	Rate, deg/sec	
Biomedical centrifuge	----------	5.0	----	---------
Cosmic dust measurement	Local vertical	1.0	0.1	Orbit rate
Microwave transmission	Local vertical	.5	.1	Orbit rate
Reflected radiation survey	Inertial	.1	.06	---------
Horizon spectrometry	Local vertical	.01	.01	1.0
Earth mapping	Orbit	.01	.001	1.12
Astronomical observations*	Inertial	.00003	----	---------

*Accuracy required for X- and Y-axes errors; Z-axis errors may be an order of magnitude greater.

It is probable that the spacecraft with its continuous and random torque disturbances (arising from operating machinery, crew motions, etc.) will not be capable of accuracies greater than 0.01° and 0.001° per second without very high control gains and excessive power consumption. A desired fine-mode accuracy of 0.01° and 0.001° per second was thus selected for this analysis. Experiments with greater accuracy requirements than these values would be mounted on a gimbaled stable platform. The gimbals would then be driven to the final accuracies while the spacecraft maintained the fine-mode accuracy.

The spacecraft is assumed to operate in three primary reference orientations while control-related experiments are performed. These orientations are orbit, local-vertical, and inertial orientation. For the orbit orientation, the Z-axis of the spacecraft is held normal to the orbit plane; the X- and Y-axes point toward the earth and along the velocity vector of the spacecraft, respectively. For the local-vertical orientation, the Z-axis of the spacecraft is alined with a local-vertical line; for the inertial orientation, the Z-axis of the spacecraft is pointed toward an inertial target such as the sun or a star image. The inertial orientation for which the spacecraft continuously points at the sun will be designated solar orientation.

Results obtained for this example spacecraft should be indicative of the controlled motion of similar orbital spacecraft, if the SIXPAC characteristics for such spacecraft are selected by the method developed in the following section.

Control-system characteristics.- Control parameters for the SIXPAC were chosen in accordance with the assumed spacecraft and experiment characteristics. To minimize the control-system weight, it was assumed that maximum slewing rates of $\pm 1.2^{\circ}$ per

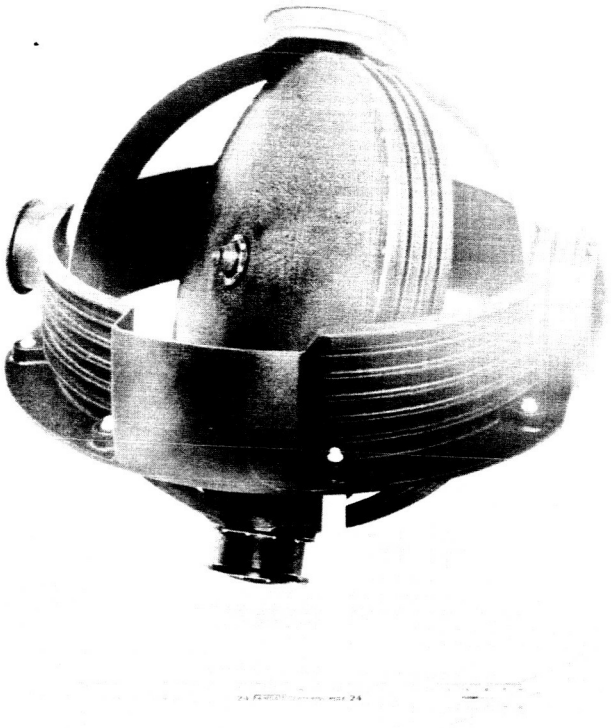

Figure 5.- Laboratory prototype of control moment gyro. L-66-4416

TABLE II.- CONTROL GAINS FOR SIXPAC

Control gains	Control mode	
	Coarse	Fine
K_1	0.675	67.5
K_2	6.75	67.5
K_3	3.375	337.5
K_4	33.75	337.5
K_5	3.3975	339.75
K_6	33.975	339.75
K_7	.525	52.5
K_8	5.25	52.5
K_9	2.625	262.5
K_{10}	26.25	262.5
K_{11}	2.6425	264.25
K_{12}	26.425	264.25

second would be required about only the Z- or minimum-inertia axis. Simultaneous maximum slewing rates about two or three axes could lead to inertial cross-coupling and corresponding sensor and control-system problems. Since the spacecraft can be readily maneuvered to any orientation, slewing about a minimum-inertia axis is thus preferable.

Angular momenta of 1,000 ft-lb-sec (1355.75 N-m-s) per gyro are adequate for the 1.2^{o} per second slewing rate and also allow simultaneous maneuver rates of about 0.5^{o} per second about all three axes. These rates should suffice for the experimental mission requirements.

Control moment gyros with angular momenta of 1,000 ft-lb-sec (1355.75 N-m-s) are currently being developed. (See refs. 7 and 8.) A laboratory prototype for such a gyro is illustrated in figure 5. This single gyro and its mounting bracket weigh approximately 130 pounds (58.97 kg) and take up about 10 cubic feet ($0.283\ m^3$) of volume. Continuous spin power of 30 watts is required to maintain the rotor speed at a constant value of 12,000 revolutions per minute.

Gains for the coarse and fine control modes were selected to give critical damping with respective time constants of 5 seconds and 0.5 second. The resultant gain values were determined by the method presented in appendix B and are given in table II.

Gimbal rate limits of 10^{o} per second were also imposed on the SIXPAC control loop to avoid excessive power consumption in case of sensor noise or large short-duration torque inputs. When this maximum rate was reached for a particular gimbal, it was automatically held until the gimbal rate command again called for a smaller rate.

Desaturation jets were assumed to have thrust levels of 50 pounds (222.4 N) with effective moment arms of 10 feet (3.048 m) for the Z-axis and 20 feet (6.096 m) for the X- and Y-axes. Time duration of the desaturation pulses was chosen as 0.50 second for the Z-axis and 0.25 second for the X- and Y-axes. The resultant gimbal desaturation should be about 10 percent of the maximum inner gimbal angle value of 70^{o}.

Coarse Control Mode

For normal operation of the spacecraft, accurate control is not necessary and attitude holds of about $\pm 5^{o}$ suffice. Disturbances for this coarse control mode may include aerodynamic and gravity-gradient torques, crew motions, docking impacts, and operation of an onboard centrifuge. Each of these disturbance types will be analyzed to assess the SIXPAC performance in providing attitude control for the spacecraft.

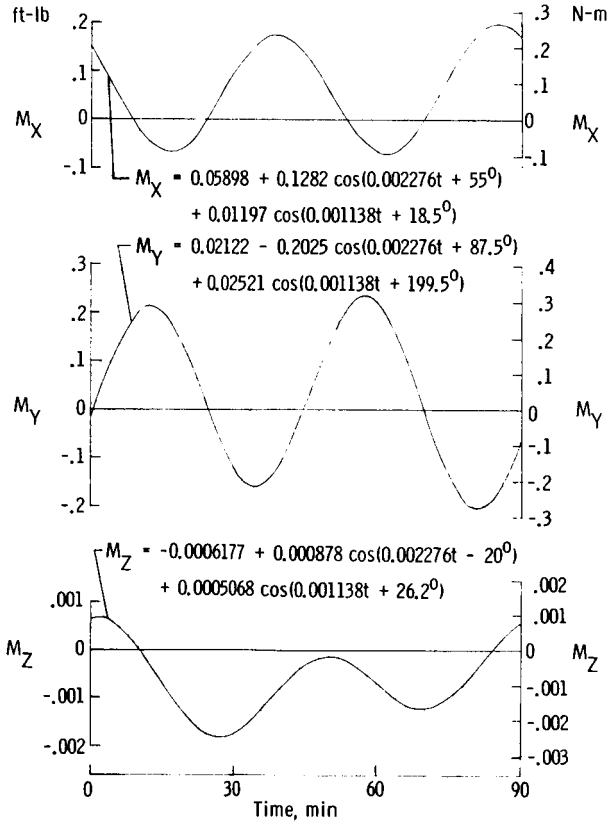

(a) Disturbance torques.

Figure 6.- Spacecraft response for characteristic aerodynamic and gravity-gradient torques in a solar orientation.

Aerodynamic and gravity-gradient torques.- Torques arising from aerodynamic drag and gravity gradients are in general biased sinusoids, such as those illustrated in figure 6(a). The torques shown in this figure were determined from a numerical solution (ref. 9) of the orbital spacecraft equations and correspond to solar orientation of the Apollo applications spacecraft. The period of the combined aerodynamic and gravity-gradient torques is equal to the orbital period of the spacecraft, and maximum torque amplitudes are approximately 0.4 ft-lb (0.54 N-m).

The controlled response of the spacecraft under these torques is presented in figure 6(b) for one orbit. The Euler angles and body rates are held to less than 0.003^{o} and 0.000005^{o} per second by the SIXPAC in its coarse control mode. The associated gimbal angles given in figure 6(c) move to

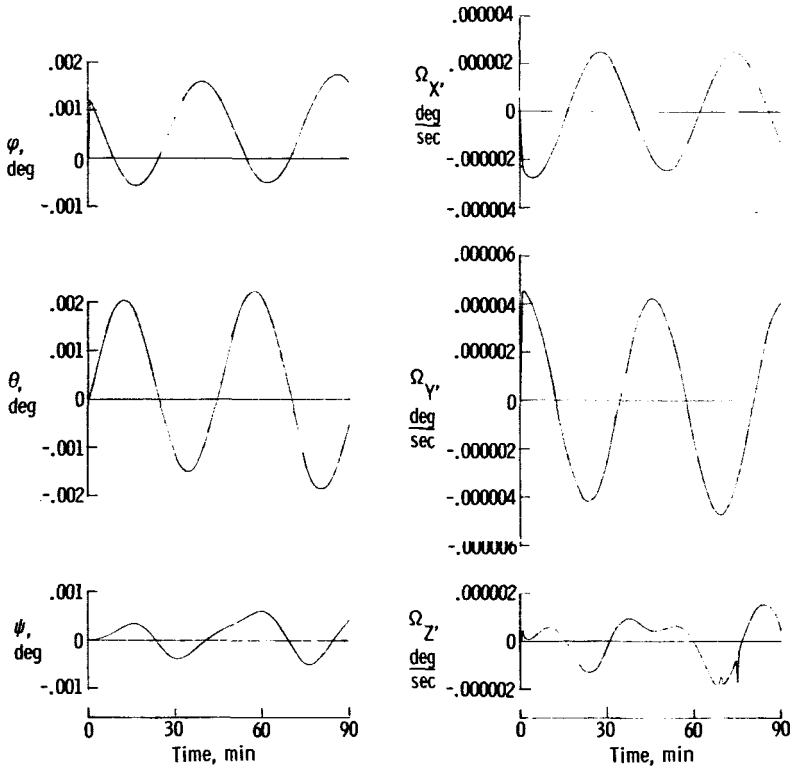

(b) Spacecraft motion.

Figure 6.- Continued.

oppose the applied torques. Since these torques have continuous biased components, the gimbal motions are slowly diverging oscillations which will eventually saturate the SIXPAC. Full desaturation would be necessary about once per day for this example. However, experimental and other disturbance requirements may increase this desaturation frequency somewhat.

Crew motions.- Crew motions within the spacecraft may be a continuous source of attitude errors. Consider, for example, the crew motion shown in figure 7(a). Here an astronaut accelerates to a constant velocity, moves once around the command service module and then stops. The resultant uncontrolled spacecraft motion, illustrated in figure 7(b), yields residual attitude errors of 1.2^{o} about the Z-axis and smaller errors about the X- and Y-axes. If the astronaut continues his motion or if more than one astronaut moves around, attitude errors due to crew motion may rapidly exceed the $\pm 5^{o}$ limits.

Figure 7(c) depicts the effects of the same motion with the SIXPAC in operation. Attitude errors are now held to less than 0.2^{o} during the motion and are damped out completely after cessation of the motion. Since the disturbances are cyclic, the gimbal angles in figure 7(d) also return to positions corresponding to a zero net momentum

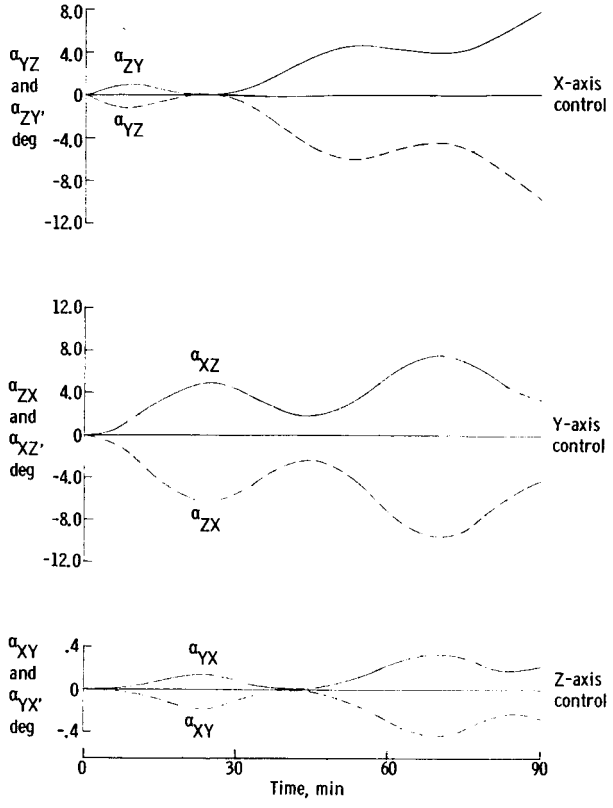

(c) Gimbal motion.

Figure 6.- Concluded.

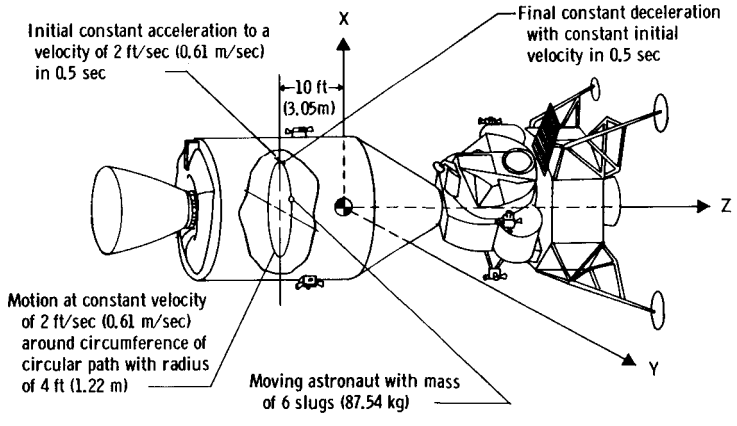

(a) Representative crew motion.

Figure 7.- Spacecraft response for a typical crew motion.

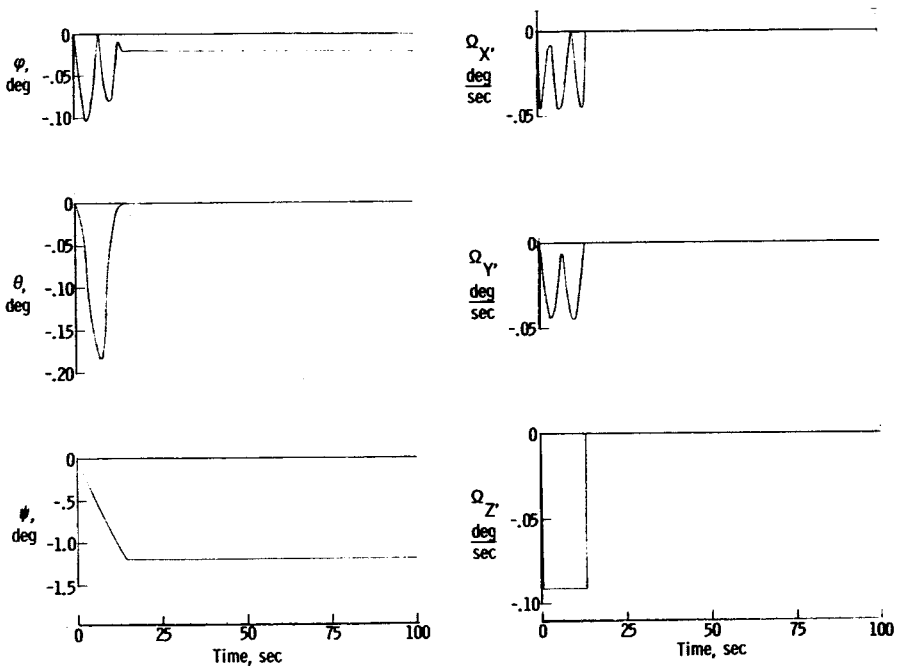

(b) Uncontrolled spacecraft motion.

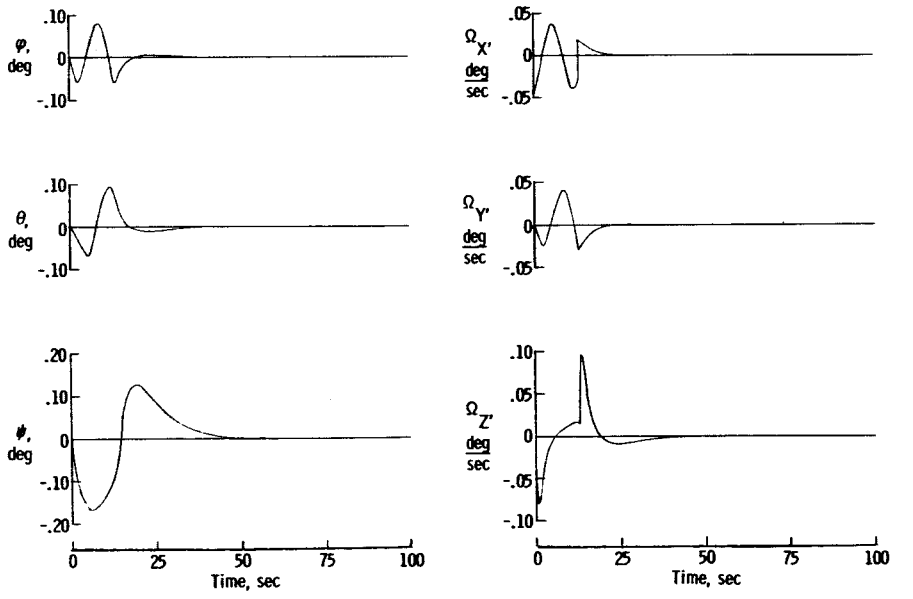

(c) Controlled spacecraft motion.

Figure 7.- Continued.

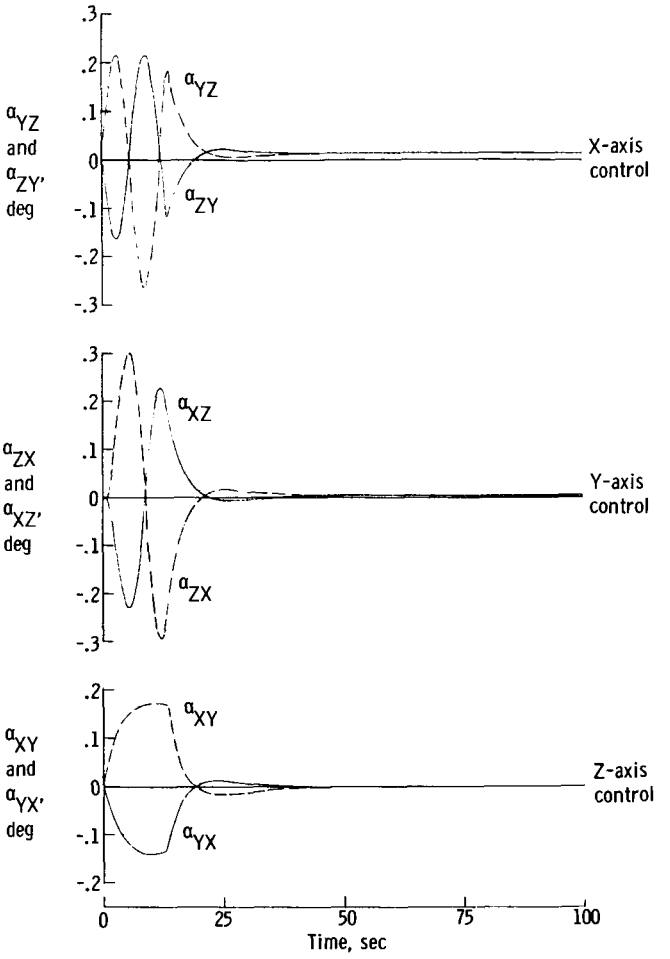

(d) Gimbal motion.

Figure 7.- Concluded.

change after completion of the motion of the astronaut. Effects of continuous mass motions are thus completely eliminated by the SIXPAC.

Docking effects.- Docking of a resupply or rendezvous vehicle with the Apollo spacecraft may result in small angular velocities of the spacecraft. Response of the spacecraft will be similar to the response for applied aerodynamic and gravity-gradient torques and is not considered here. However, it should be noted that the docked vehicle may produce large changes in the inertias of the Apollo applications spacecraft. The control gains for the SIXPAC may thus have to be changed to correspond to these new inertias, if rapid and accurate control of the spacecraft is required.

Centrifuge operation.- A possible biomedical experiment for the Apollo applications spacecraft is a centrifuge, such as that shown in figure 8(a). Spin-up and despin torques

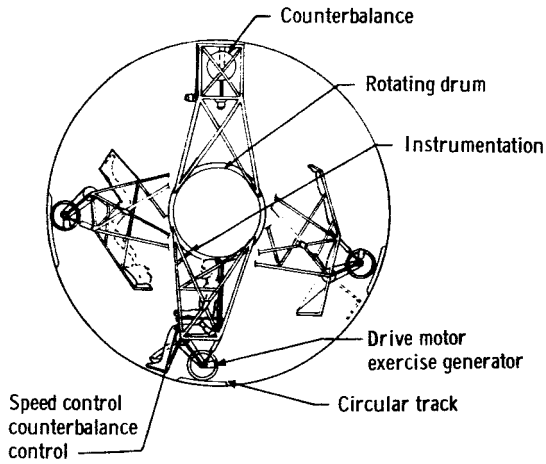

(a) Sketch of centrifuge.

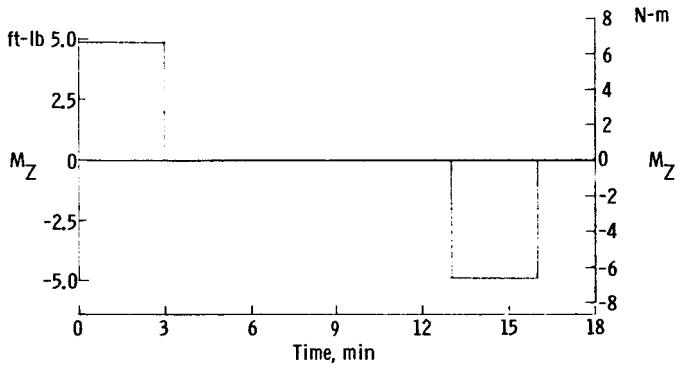

(b) Centrifuge torques.

Figure 8.- Simulation of centrifuge experiment for spacecraft.

for this centrifuge are 4.75 ft-lb (6.44 N-m) and are applied for 3 minutes, as shown in figure 8(b). Since the 16-minute total operation of the centrifuge will produce a 980° rotation of the spacecraft about the centrifuge axis, compensating control torques must be provided for this experiment. The corresponding spacecraft response with the SIXPAC is presented in figure 8(c). Attitude errors of the spacecraft are held to 0.3° during operation of the centrifuge. Since the centrifuge torques are cyclic, the SIXPAC gimbal angles in figure 8(d) return to their reference position after completion of the experiment.

As seen from these examples, the SIXPAC is capable of stabilizing the spacecraft to well within ±5° in its coarse mode. Average power consumption for these typical disturbances was about 90 watts, and desaturation fuel should be required only to compensate for biased aerodynamic and gravity-gradient torques.

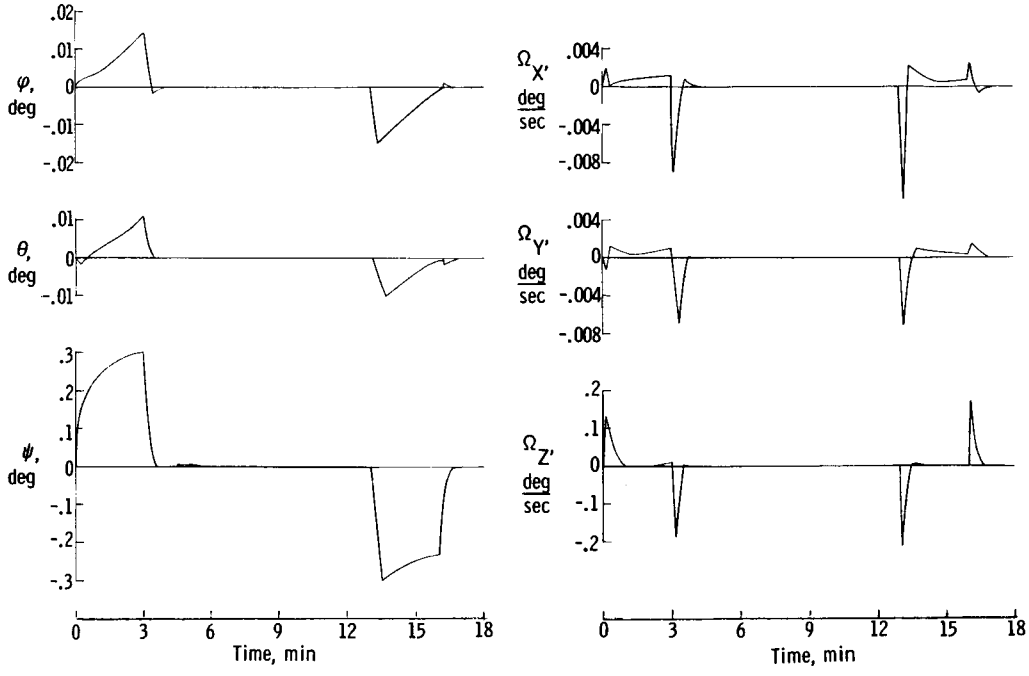

(c) Spacecraft motion.

Figure 8.- Continued.

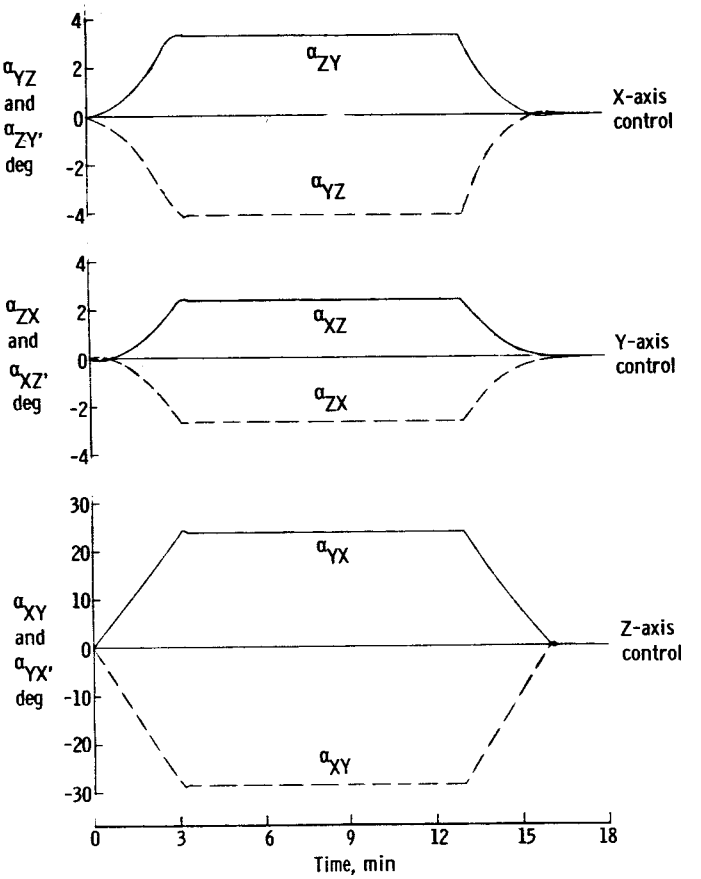

(d) Gimbal motion.

Figure 8.- Concluded.

Fine Control Mode

When experiments requiring fine attitude control of the Apollo spacecraft are to be performed, the SIXPAC must be switched to its fine control mode. Crew motions should now be restricted to take place very slowly and centrifuge and docking operations are suspended. Aerodynamic and gravity-gradient torques will, of course, continue to act on the spacecraft.

The primary task of the control system in this mode is the performance of the maneuvers and attitude and rate holds necessary for successful experiment operation. This objective must be carried out while aerodynamic, gravity-gradient, and other low-level torques are acting on the spacecraft.

Maneuvers.- Maneuvers of the spacecraft are necessary to acquire the desired pointing attitude for the spacecraft experiments. Several maneuvers may thus take place daily.

For the simulation of maneuvers, small disturbance torques acting on the spacecraft are assumed to be negligible. The control problem is then reduced to a commanded reorientation or a commanded rate about the spacecraft axes.

The SIXPAC provides maneuver capability by commanding constant spacecraft Euler rates in the gimbal control laws. In the actual spacecraft, this procedure would require the computation of the desired spacecraft body rates and the associated Euler angles and rates. The gimbal rates are commanded to follow the difference between the computed values and the actual spacecraft attitude and rates. The maneuver is completed when this difference is reduced to zero after the desired spacecraft rates or attitude have been reached. The gimbal control laws needed for these maneuvers are developed in appendix B.

Several typical spacecraft maneuvers are presented in figures 9 and 10. Figure 9 illustrates consecutive 45° maneuvers about the three spacecraft axes. These maneuvers were accomplished by commanding a rate about a spacecraft axis, holding this rate until the desired attitude was reached, and then damping out the commanded rate. Successive completion of this process for the Z-, Y-, and X-axes allows any desired spacecraft orientation to be attained. Care should be taken to limit the maximum rates during this maneuver to avoid saturation of the SIXPAC.

For figure 9 a 1° per second Euler rate was commanded about the Z-axis, was held for 45 seconds, and then was commanded to zero. Similar maneuvers with 0.5° per second Euler rates were carried out about the Y- and X-axes. The final orientation of the spacecraft was achieved in 225 seconds. The residual gimbal angles, seen in figure 9(b) after completion of the maneuver, are due to the inertial cross-coupling torques of the

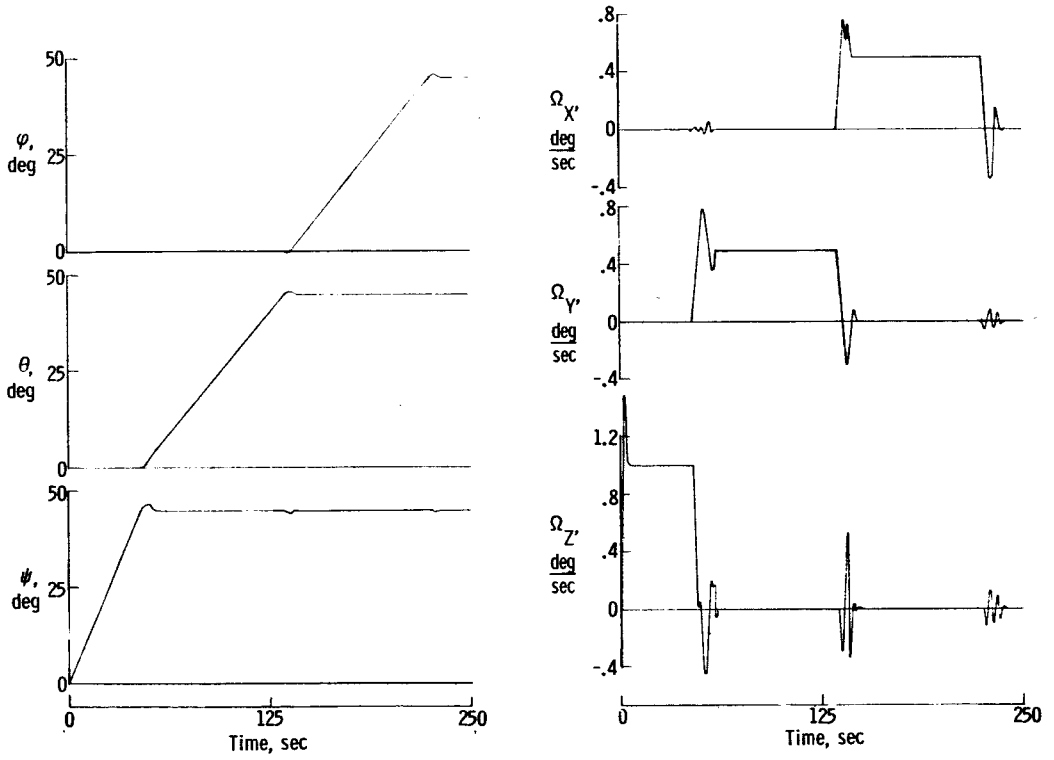

(a) Spacecraft motion.

Figure 9.- Consecutive 45^{0} maneuvers about the spacecraft axes.

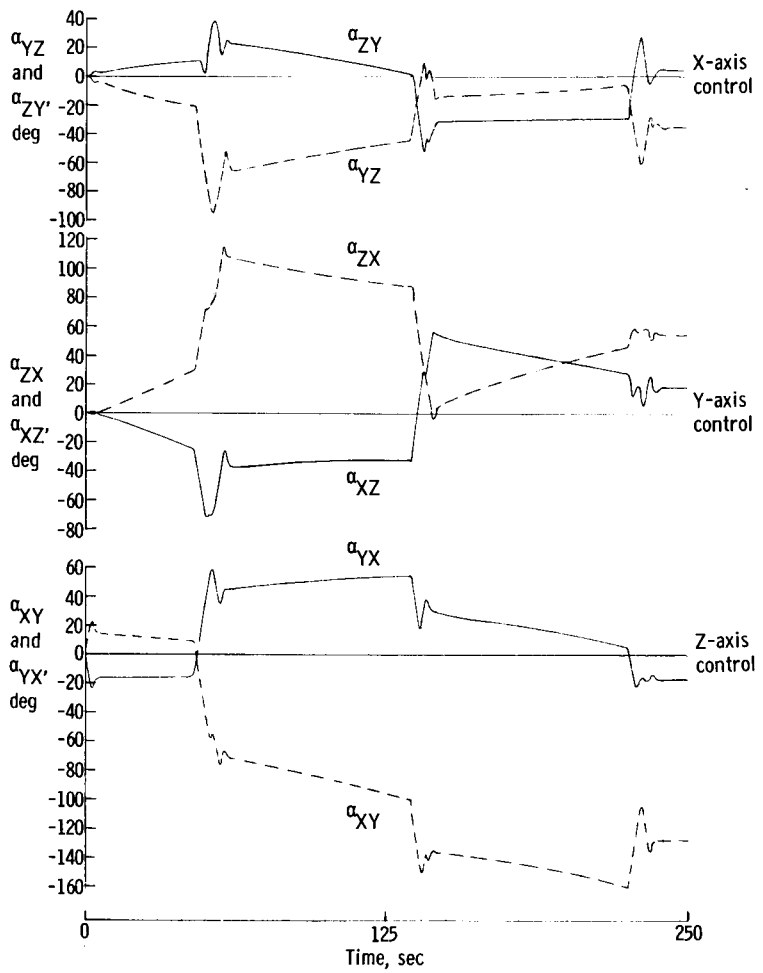

(b) Gimbal motion.

Figure 9.- Concluded.

spacecraft during the maneuver. No desaturation fuel was used for the maneuver and the average theoretical power consumption was 111 watts.

Figure 10 depicts a simultaneous 45° maneuver about all three spacecraft axes. This maneuver was performed by commanding spacecraft body rates corresponding to constant Euler rates of 0.5° per second, holding these body rates until the desired Euler angles were reached, and then driving the Euler rates to zero. Reorientation of the spacecraft required about 90 seconds and was performed with an average theoretical power consumption of 150 watts. Again, desaturation was not necessary.

Since the final attitude of the spacecraft in these maneuvers is dependent only on the length of the time interval during which the commanded body or Euler rates are held constant, the spacecraft response shown in figures 9 and 10 is typical of that to be expected for all maneuvers.

Rendezvous and resupply operations.- In addition to performing simple reorientation maneuvers, the SIXPAC may also have to perform more complex control tasks associated with resupply and rendezvous operations. Consider, as an example, a resupply operation where a small unmanned vehicle housing replacement parts or emergency supplies is launched to rendezvous with the Apollo applications spacecraft. Terminal

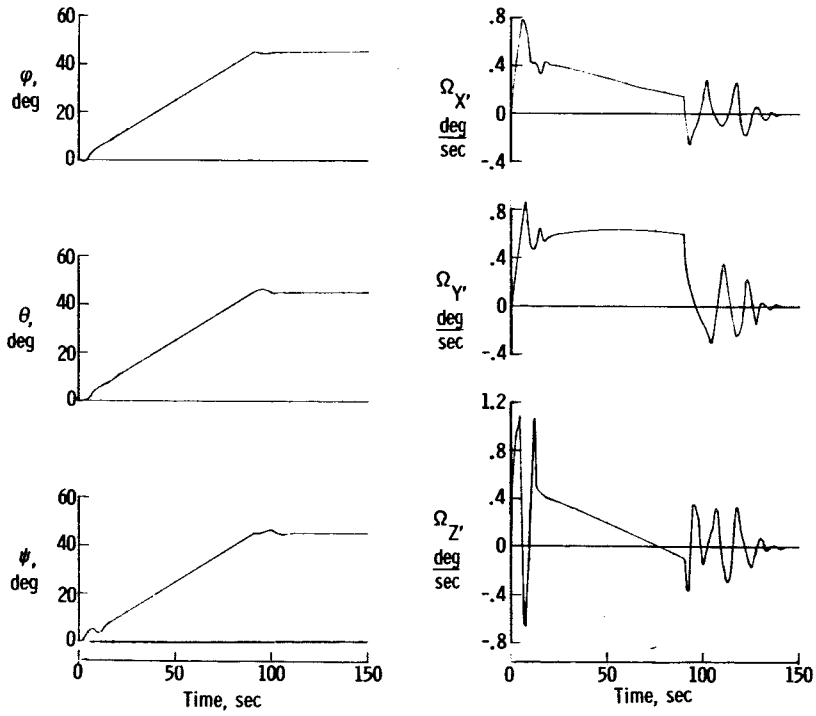

(a) Spacecraft motion.

Figure 10.- Simultaneous 45° maneuvers about the spacecraft axes.

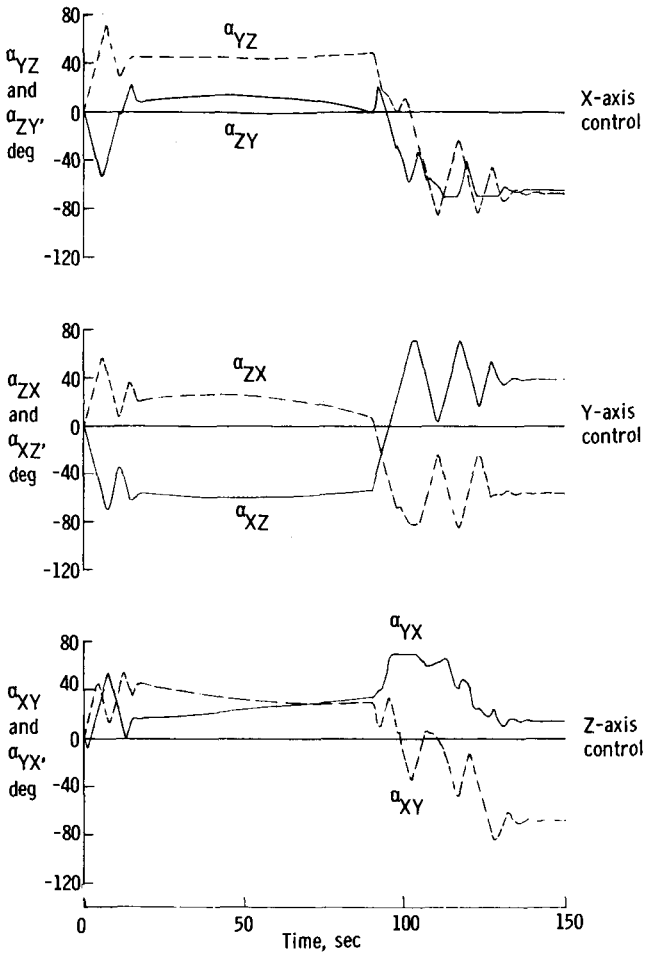

(b) Gimbal motion.

Figure 10.- Concluded.

guidance and control of this resupply vehicle is to be provided by the Apollo crew, and the spacecraft must track the resupply vehicle during the final portion of its ascent orbit.

The analytical simulation for such a tracking mission may be derived from the simplified mathematical model of figure 11(a). This model of the resupply operation approximates the ascent orbit of the resupply vehicle by a Hohmann ellipse in geocentric coordinates. The ascent orbit and the circular spacecraft orbit are assumed to be coplanar. Launch of the resupply vehicle is to be timed so that the spacecraft and the resupply vehicle simultaneously reach their rendezvous position.

The spacecraft will maneuver until the sensor reference for its X-axis acquires the resupply vehicle in its field of view, while the Y-axis is held in the orbit plane. Tracking of the resupply vehicle is then initiated by commanding the spacecraft X-axis to point continuously at the resupply vehicle.

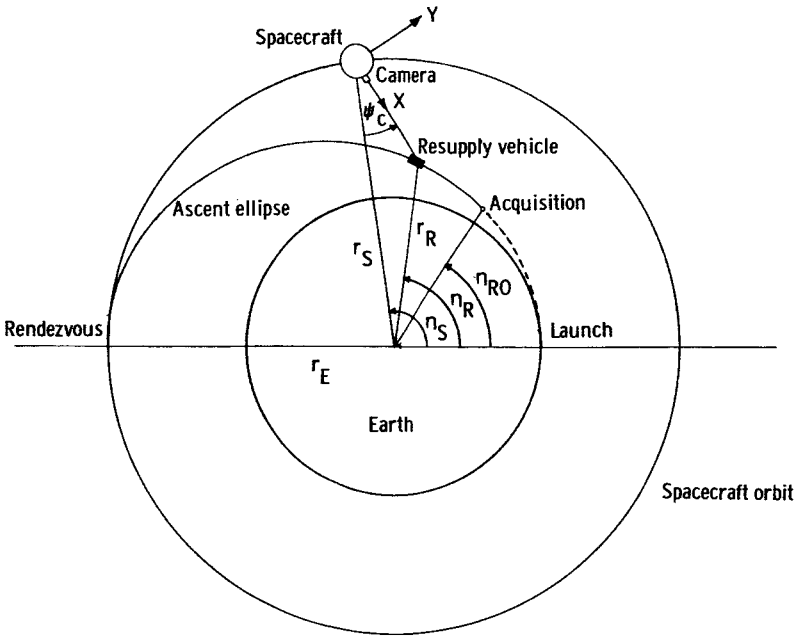

(a) Mathematical experiment model.

Figure 11.- Simulation of resupply operations for spacecraft.

The computer simulation of this tracking maneuver requires the development of a desired tracking rate about the Z-axis of the spacecraft. In terms of the orbit radius r_S of the spacecraft and angular position η_S and of the radial position r_R of the resupply vehicle and true anomaly η_R, this tracking rate can be derived as

$$\left.\begin{aligned} \Omega_{Ze} &= \frac{r_R^2\left(\dot{\eta}_R - \dot{\eta}_S\right) - r_S\left[r_R\left(\dot{\eta}_R - \dot{\eta}_S\right)\cos\left(\eta_R - \eta_S\right) + \dot{r}_R \sin\left(\eta_R - \eta_S\right)\right]}{r_R^2 + r_S^2 - 2r_R r_S \cos\left(\eta_R - \eta_S\right)} && \left(r_R \neq r_S\right) \\ \Omega_{Ze} &= 0 && \left(r_R = r_S\right) \end{aligned}\right\} \quad (1)$$

where

$$\dot{\eta}_R = \left[\left(\frac{r_E + r_S}{2r_E r_S}\right)^3 \mu\right]^{1/2} \left(1 + e\cos\eta_R\right)^2 \quad (2)$$

$$\eta_R = \eta_{R0} + \int^t \dot{\eta}_R \, dt \quad (3)$$

$$\dot{r}_R = e\left[\frac{\mu}{r_E(1+e)}\right]^{1/2} \sin \eta_R \tag{4}$$

$$r_R = \frac{r_E(1+e)}{1 + e \cos \eta_R} \tag{5}$$

$$e = \frac{r_S - r_E}{r_S + r_E} \tag{6}$$

$$\dot{\eta}_S = \left(\frac{\mu}{r_S^3}\right)^{1/2} \tag{7}$$

$$\eta_S = \eta_{S0} + \dot{\eta}_S t \tag{8}$$

The quantities e, r_E, and μ denote the ascent orbit eccentricity, the radius of the earth, and the gravitational parameter of the central force field of the earth, respectively.

After initial acquisition of the resupply vehicle, one has

$$\psi_{c0} = \tan^{-1} \frac{r_{R0} \sin\left(\eta_{R0} - \eta_{S0}\right)}{r_{R0} \cos\left(\eta_{R0} - \eta_{S0}\right) - r_S} \tag{9}$$

with the terms μ, r_E, r_S, η_{R0}, and η_{S0} specified as input to the computer simulation. Values of r_{R0}, η_{R0}, and η_{S0} should be selected to allow simultaneous attainment of the target position.

For an example resupply mission, these quantities were chosen as

$$r_{R0} = 3{,}440 \text{ n. mi.} = 6{,}371 \text{ km}$$

$$\eta_{R0} = 0^o$$

$$\eta_{S0} = 7.373^o$$

with

$$\mu = 62{,}746.8 \text{ n. mi.}^3/\text{sec}^2 = 398{,}579.1 \text{ km}^3/\text{sec}^2$$

$$r_E = 3{,}440 \text{ n. mi.} = 6{,}371 \text{ km}$$

$$r_S = 3{,}640 \text{ n. mi.} = 6{,}741 \text{ km}$$

for the 200-nautical-mile (370-km) earth orbit. It is thus assumed that the spacecraft acquires the resupply vehicle in its field of view at launch and tracks it continuously until rendezvous is effected. The resultant spacecraft and SIXPAC response is shown in figure 11.

Figure 11(b) illustrates the rate and attitude of the spacecraft about the Z-axis. The spacecraft is initially maneuvered to acquire the resupply vehicle at launch, and completes the associated 62° maneuver in approximately 1 minute. Tracking of the resupply vehicle then commences and is continued until the resupply vehicle achieves the

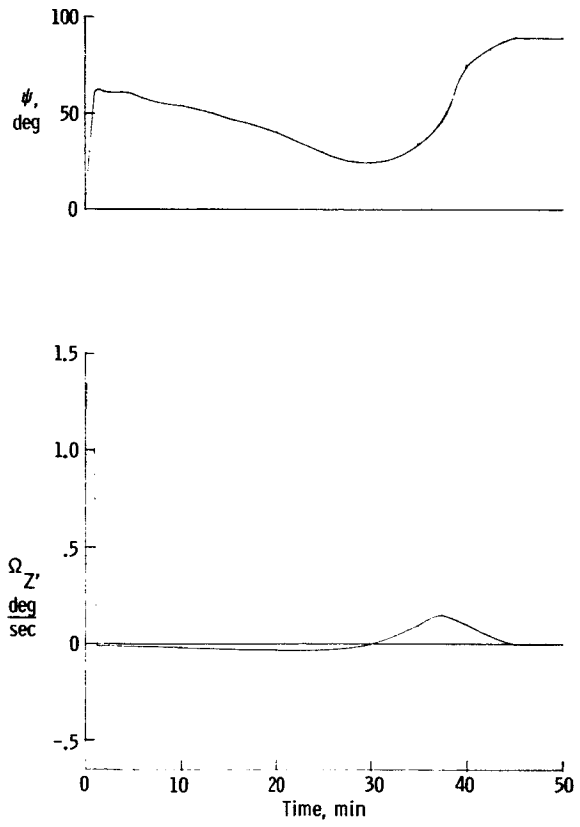

(b) Tracking angle and rate.

Figure 11.- Continued.

orbit of the spacecraft. At this time, the tracking rate Ω_Z is driven to zero and the tracking angle ψ approaches 90^o. The entire resupply operation takes about 46 minutes.

The spacecraft rate and attitude errors and the SIXPAC gimbal motions for this operation are presented in figure 11(c) and figure 11(d), respectively. No desaturation fuel was required for the tracking maneuvers, and the average power consumption was 90 watts.

It should be noted that the simplified simulation model used for the resupply operation and the models used to simulate later experiments are only idealized approximations to the anticipated experiment tasks. These models do, however, serve to demonstrate the theoretical capacity of the SIXPAC for performing typical control tasks associated with the experimental mission.

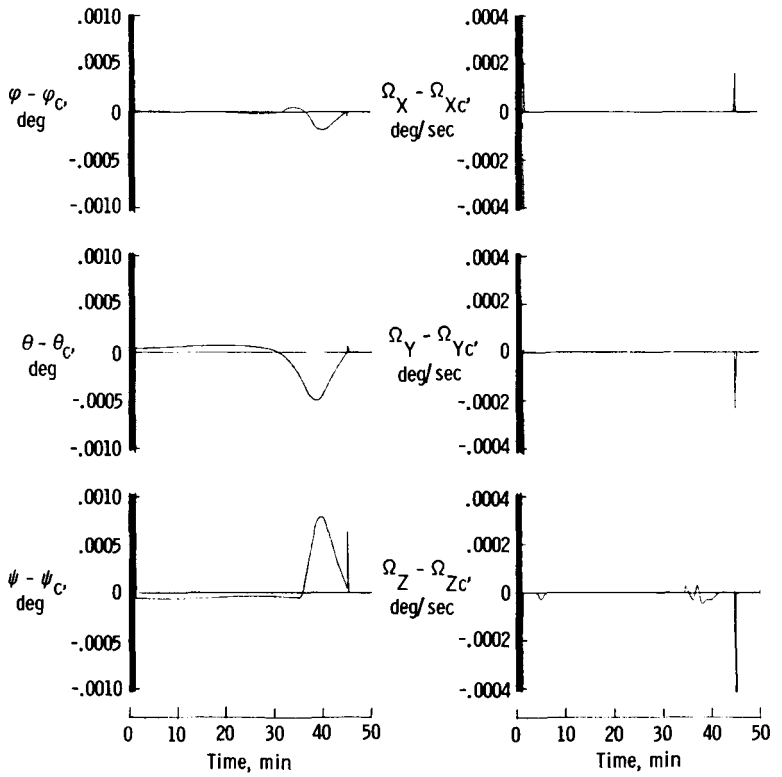

(c) Attitude and rate errors.

Figure 11.- Continued.

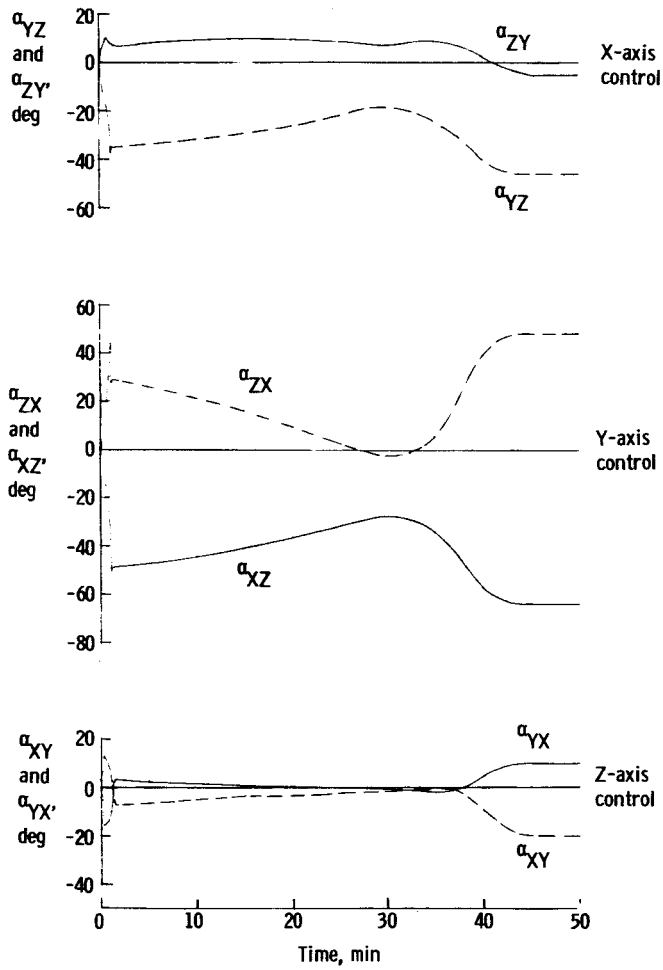

(d) Gimbal motion.

Figure 11.- Concluded.

Earth mapping experiment.- Earth mapping and photography may be an important task for future manned orbital missions. A typical earth observation and mapping experiment is correspondingly sketched in figure 12(a). For this experiment, the spacecraft is maneuvered so that a camera pointing along its X-axis tracks a target point on the surface of the earth. The target point is acquired at the horizon and is then tracked continuously. For the present simulation, aerodynamic and gravity-gradient torques act on the spacecraft throughout the experiment. The associated disturbance torque histories are shown in figure 12(b).

The necessary tracking rate Ω_{Ze} may be derived as

$$\Omega_{Ze} = \frac{r_E \dot{\eta}_S (r_S \sin \eta_S - r_E)}{r_S^2 - 2r_S r_E \sin \eta_S + r_E^2} \tag{10}$$

by referring to figure 12(a). Tracking is assumed to begin at the horizon where

$$\psi_{c0} = \sin^{-1} \frac{r_E}{r_S} \tag{11}$$

and ends when the target point disappears over the opposite horizon. Rate accuracies of 0.001^o per second and attitude accuracies of 0.01^o about all three axes must be maintained during the earth mapping experiment.

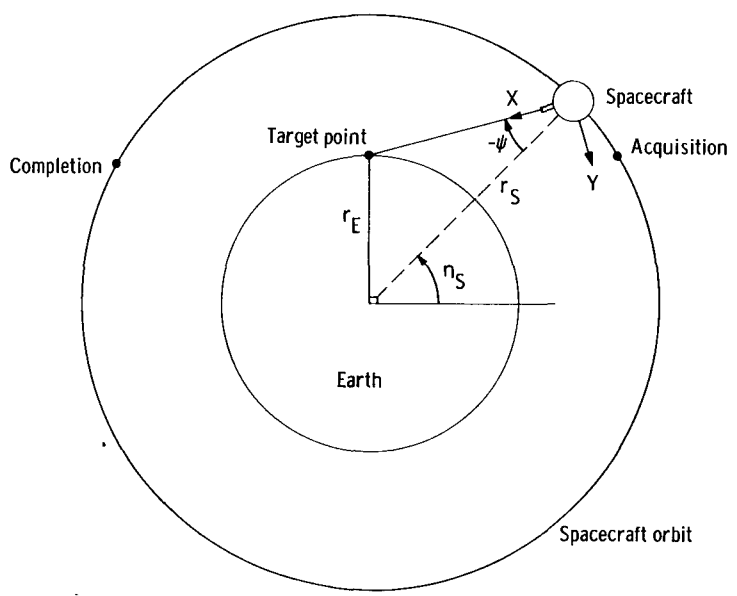

(a) Mathematical experiment model.

Figure 12.- Simulation of earth-mapping experiment.

Figure 12(c) presents the controlled spacecraft motion about the Z-axis. A maneuver to $\psi_{c0} = -72^{o}$ acquires the target in approximately 1.2 minutes. The earth tracking rate is then commanded from zero to a maximum of 1.12^{o} per second, when ψ_c is zero and the target is directly below the spacecraft. As the target passes toward the opposite horizon, the tracking angle goes to $-\psi_{c0}$ and the tracking rate tends toward zero. About 10 minutes were required for this simulated experiment.

The spacecraft errors and the SIXPAC gimbal angles are illustrated in figures 12(d) and 12(e). As seen from figure 12(d), the rate errors were held to less than 0.001^{o} per second and attitude errors were less than 0.01^{o} during the tracking mission. The SIXPAC performance is thus more than adequate for the pointing requirements of the experiment. The gimbal angles, given in figure 12(e), did not attain their limiting values and correspondingly were not desaturated. The average theoretical power consumption for the experiment was 91 watts.

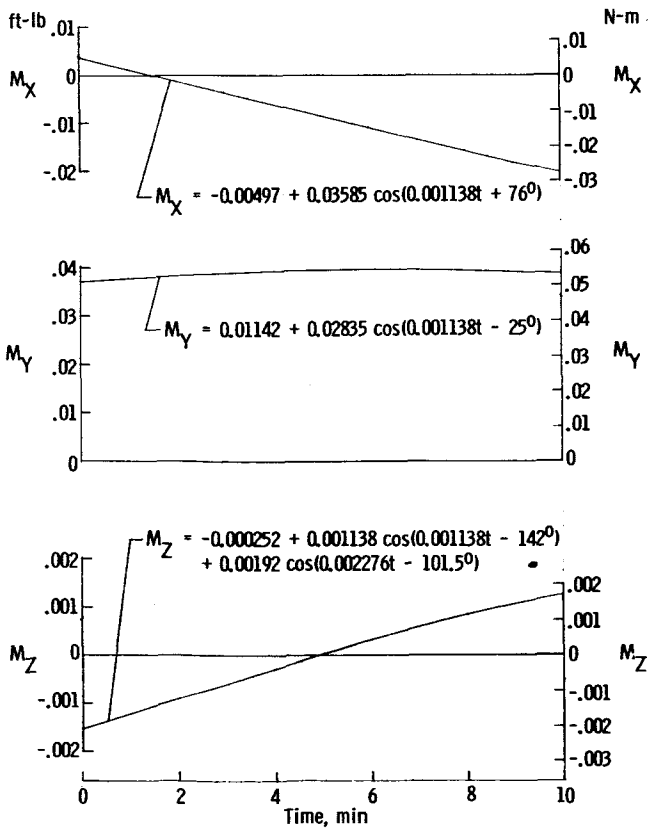

(b) Disturbance torques for orbit orientation.

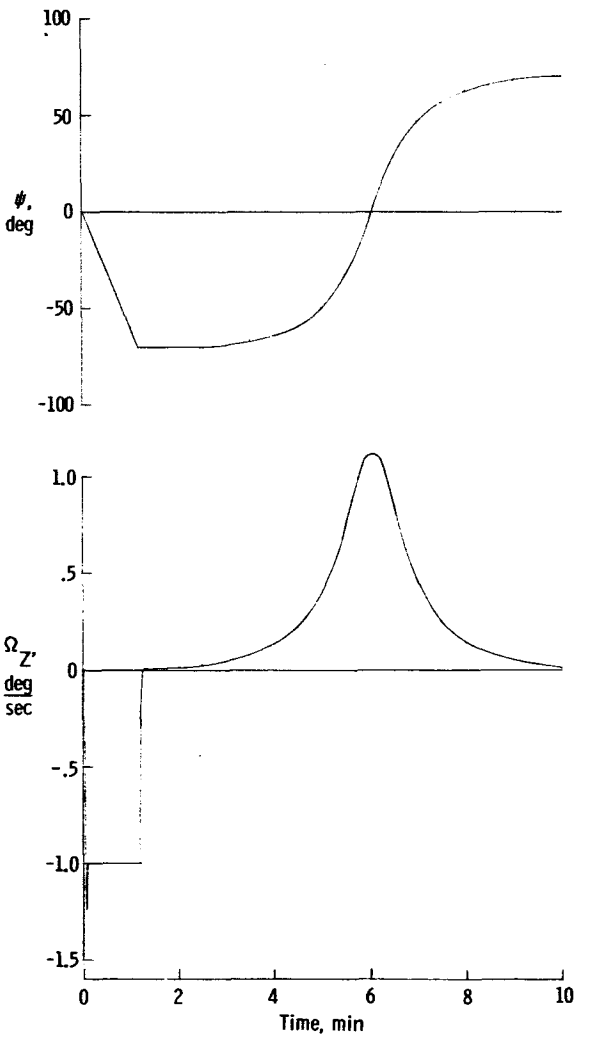

(c) Tracking angle and rate.

Figure 12.- Continued.

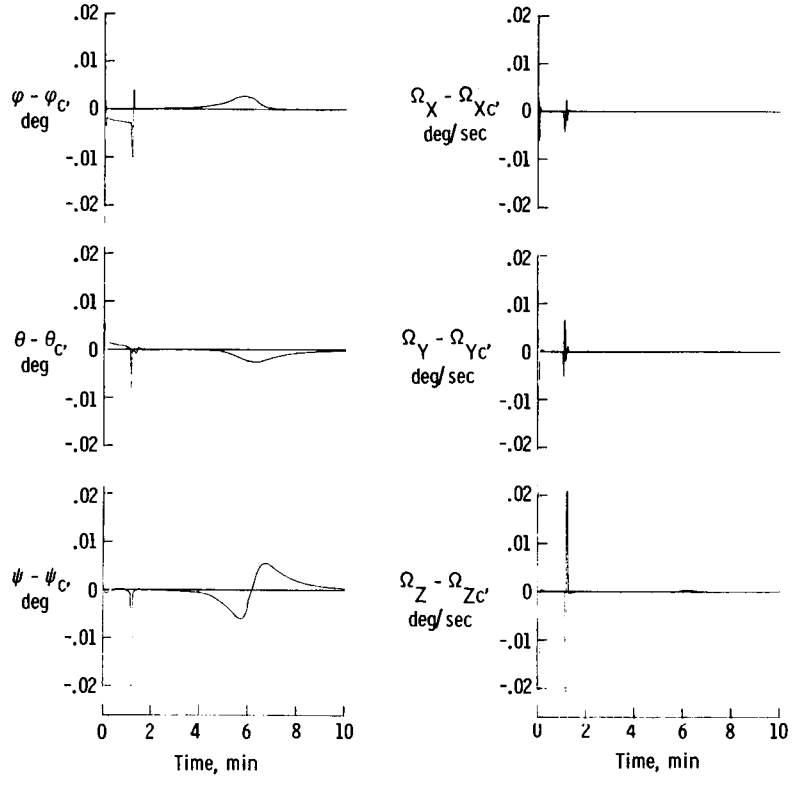

(d) Attitude and rate errors.

Figure 12.- Continued.

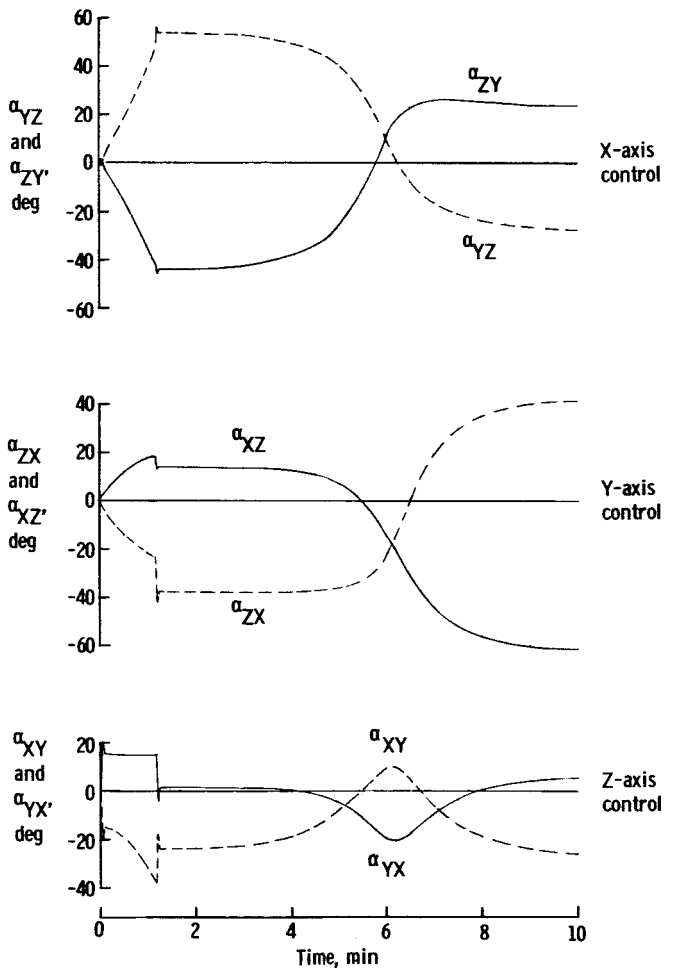

(e) Gimbal motion.

Figure 12.- Concluded.

Horizon spectrometry experiment.- Another experiment under consideration is horizon spectrometry or the study of the atmosphere immediately above the horizon of the earth. The Z-axis of the spacecraft is now alined with the local vertical and points toward the earth, as shown in figure 13(a). A camera in the spacecraft is pointed at the horizon and the vehicle rotates about an axis normal to the orbit plane at orbit rate to keep the horizon in sight. Slewing rates $\dot{\eta}_T$ of 1^o per second are simultaneously commanded about the negative Z-axis to allow observation of the complete horizon about the periphery of the earth in a short period of time. Pointing and tracking accuracies of 0.01^o are specified for this experiment.

The required tracking rates become

$$\Omega_{Xe} = \dot{\eta}_S \cos \dot{\eta}_T t = 0.0654 \cos t$$

$$\Omega_{Ye} = -\dot{\eta}_S \sin \dot{\eta}_T t = 0.0654 \sin t$$

$$\Omega_{Ze} = \dot{\eta}_T = -1.0$$

where the initial values of the tracking angles are taken as zero.

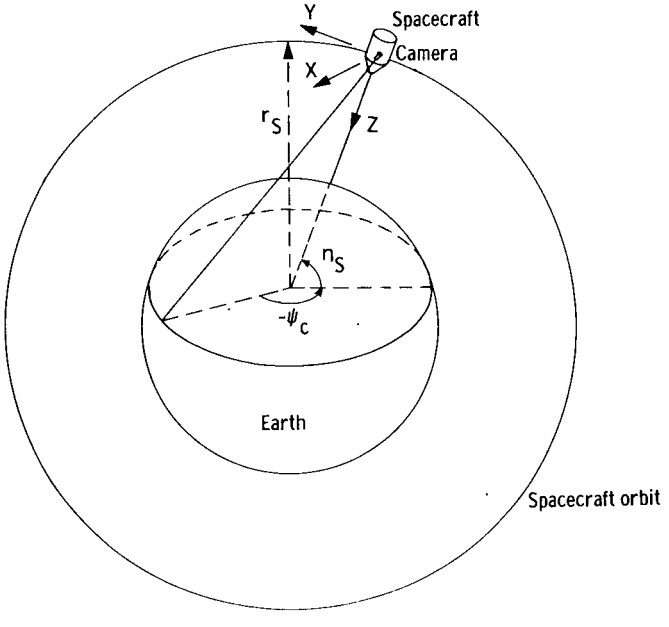

(a) Mathematical model of horizon spectrometry experiment.

Figure 13.- Simulation of horizon spectrometry experiment.

Aerodynamic and gravity-gradient torques that act on the spacecraft were approximated by the torque histories presented in figure 13(b) for the local vertical orientation. These torques were applied continuously during the horizon spectrometry experiment.

The motion of the spacecraft for the experiment is illustrated in figure 13(c). The complete scan circuit of the periphery of the earth required about 6 minutes. Errors from the commanded spacecraft motion during these maneuvers are given in figure 13(d); it may be seen that the required pointing accuracies of 0.01^{o} were obtained for all spacecraft axes. The gimbal angles, shown in figure 13(e), did not saturate in this experiment simulation so that no reaction jet fuel was required. Average power consumption for the horizon spectrometry experiment was about 91 watts.

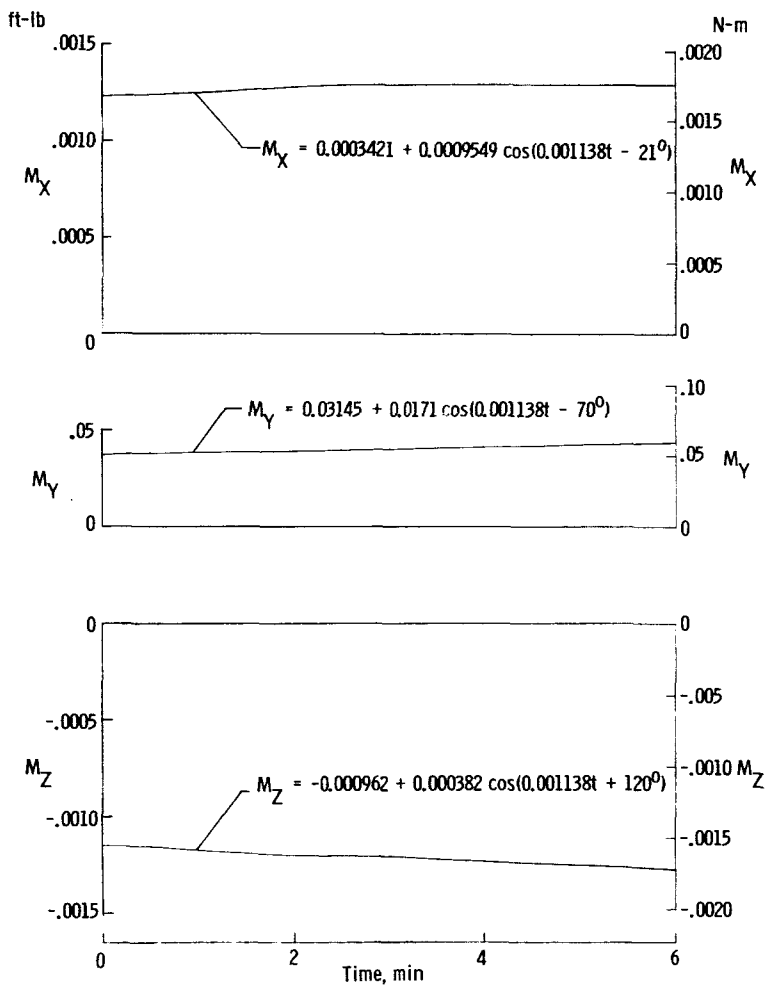

(b) Disturbance torques for local vertical orientation.

Figure 13.- Continued.

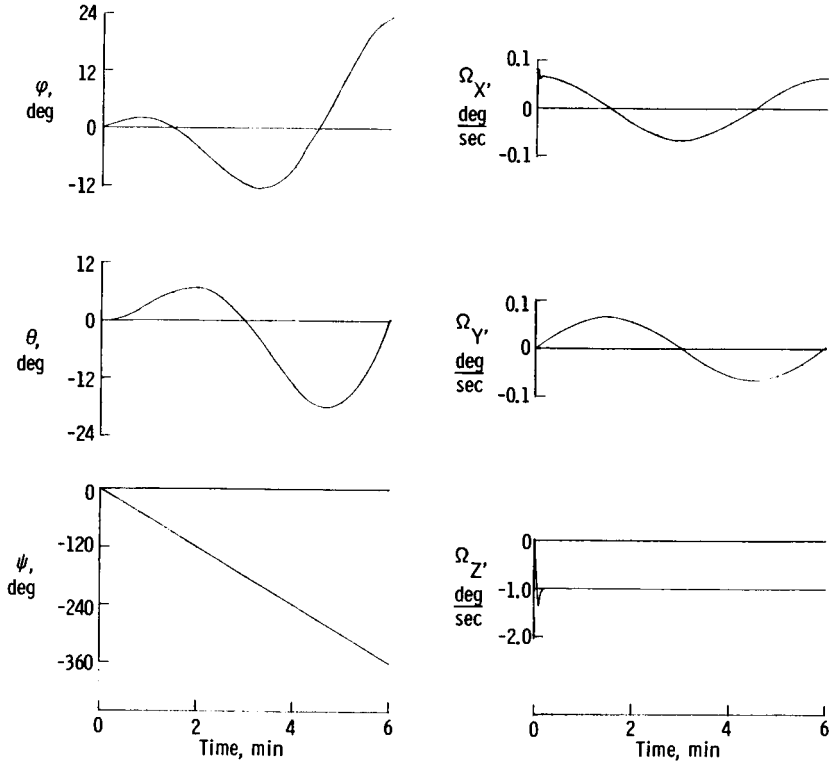

(c) Spacecraft motion.

Figure 13.- Continued.

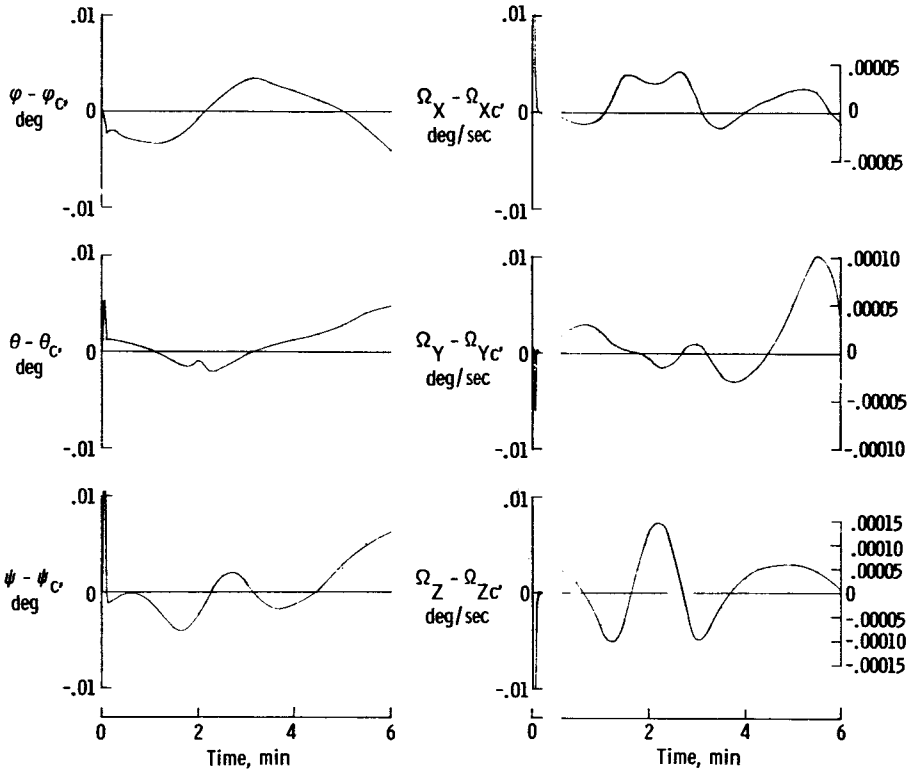

(d) Attitude and rate errors. (For rate errors, ordinate scale shifts from left to right of graph after 0.2 minute.)

Figure 13.- Continued.

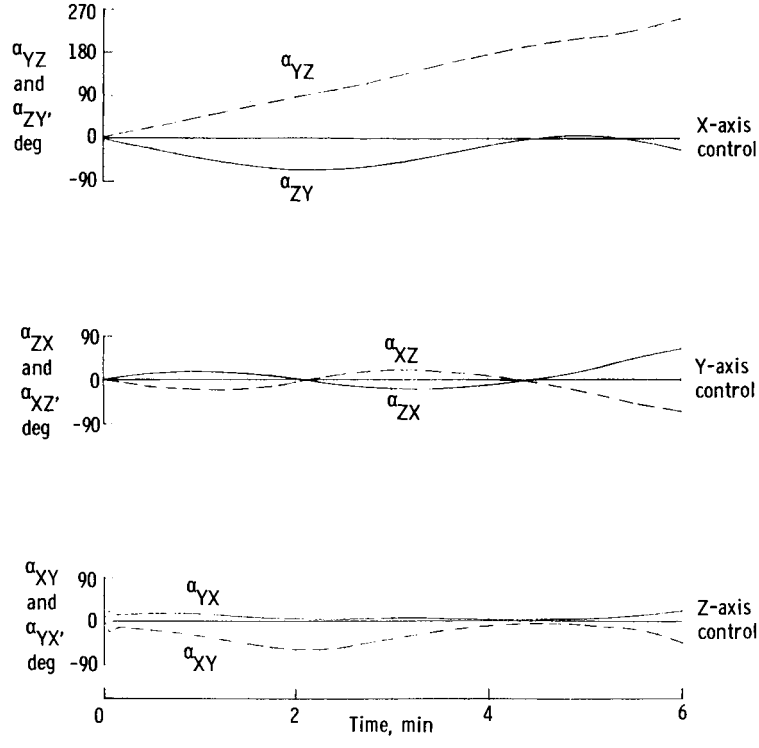

(e) Gimbal motion.

Figure 13.- Concluded.

Telescope experiment.- A manned telescope is the final experiment which will be considered in this analysis. Optical-axis stabilization approaching 0.1 arc second will be necessary while the telescope, which is alined with the spacecraft Z-axis, points toward a target star. To achieve this accuracy, the telescope may have to be isolated from the spacecraft by gimbaling of the optics within the telescope or by mounting of the telescope on a gimbaled stable table with a self-contained stabilization system. A smaller version of SIXPAC may then be feasible for control of the gimbaled telescope.

No attempt to simulate the entire telescope dynamics is made herein. Instead, the telescope experiment, as illustrated in figure 14(a), is crudely represented by a constant commanded inertial orientation with applied torques represented by the typical aerodynamic and gravity-gradient torques of figure 6(a). The controlled spacecraft motion under these relatively large disturbance torques should serve to indicate maximum accuracies that may be expected from the SIXPAC in an inertial hold condition.

For the computer simulation of this inertial orientation hold, the Z-axis of the spacecraft is thus pointed at the sun and is required to hold that inertial attitude. The position and rate errors of the spacecraft in the presence of the external disturbance torques are given in figure 14(b). It may be seen that attitude holds to within 0.1 arc second for the three spacecraft axes are theoretically attained with the SIXPAC. Actual accuracies are, of course, dependent on the degree to which the theoretical SIXPAC model can be represented by realistic hardware. Experimental research with the SIXPAC must thus precede any use of this system for such extremely fine attitude control.

The gimbal angles, shown in figure 14(c), remained small throughout the experiment. Power consumption was correspondingly small and an average of 90 watts was required.

Control implementation.- One should note that the implementation of the SIXPAC control scheme will be simpler in actual flight than in these computer simulations. The mechanization of the control commands would require only the computation of desired maneuver-rate buildups and decays. All other experimental tasks, such as earth tracking or inertial holds, can be performed by measuring the errors between the desired and the actual attitudes and rates. These errors are then used directly in the formulation of the needed gimbal rates. For a characteristic experimental task, the spacecraft is first maneuvered to acquire its target and is then required to track that target. Both manual and automatic control appear to be feasible for SIXPAC operation onboard the spacecraft.

The preceding control tasks for the experiments can be considered to be typical of the tasks a control system for future manned spacecraft may have to perform. The SIXPAC was able to accomplish all these tasks with relatively low power consumption, and thus appears to be well suited for application to manned spacecraft with complex experimental missions.

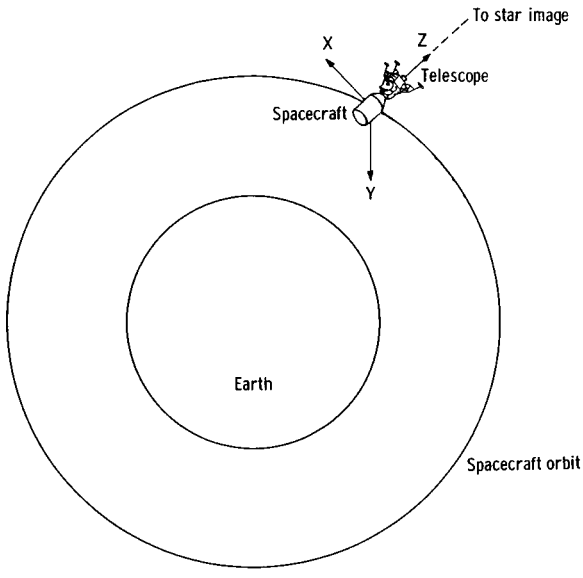

(a) Mathematical experiment model.

Figure 14.- Simulation of manned telescope experiment.

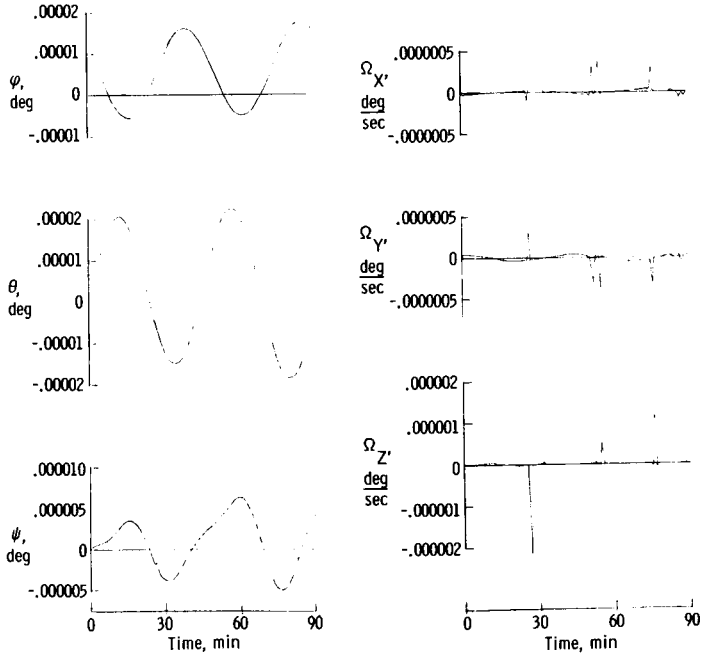

(b) Rate and attitude errors.

Figure 14.- Continued.

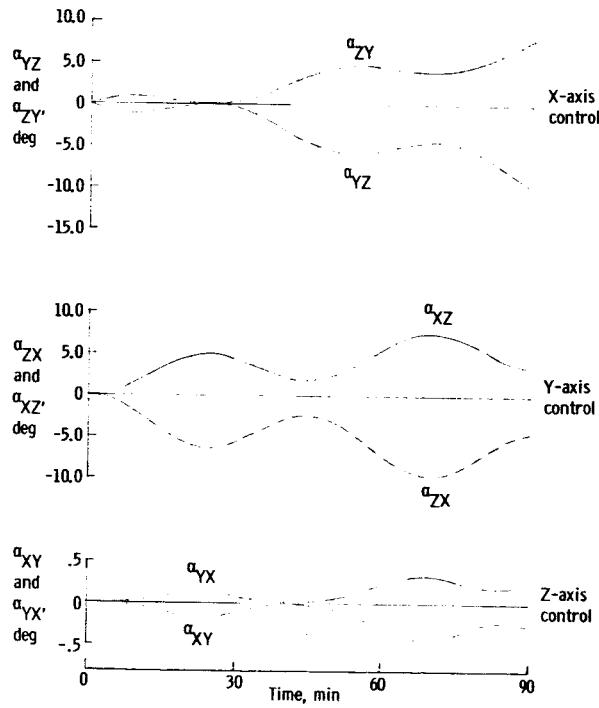

(c) Gimbal angles.

Figure 14.- Concluded.

Desaturation and Failure Modes

No desaturation was required for the example control tasks considered in this analysis. In actual operation of the SIXPAC, biased disturbance torques may, however, cause occasional saturation of the gimbal angles. A desaturation technique for the SIXPAC gyros must thus be developed and evaluated.

Desaturation technique.- A relatively simple desaturation scheme was selected for use with the SIXPAC. For this scheme mechanical stops are provided at a limiting inner gimbal angle, which was chosen as $\pm 70^{\circ}$ for the present analysis. As this gimbal angle is approached for a particular gyro, the stops automatically slow the gyro and stop it at its limiting value. A constant-amplitude torque pulse is then applied about the control axis of the spacecraft, when the inner gimbal angle corresponding to that axis becomes saturated while additional control torques are required. The amplitude and duration of the torque pulse are selected to reduce the corresponding inner and outer gimbal angle magnitudes by a specified percentage, in general, by about 10 percent of the limiting value. The gimbals are automatically commanded to counteract the torque pulse and thus are desaturated. This scheme may not yield minimum fuel and power consumption during the desaturation mode; it should, however, suffice to demonstrate the operation of the SIXPAC in both normal and desaturation modes. Additional discussion of the mechanization and computer simulation of this desaturation technique is given in appendix B.

More complex desaturation schemes requiring additional sensor checking and variable pulse width desaturation torques also appear to be possible and should result in further desaturation fuel savings. The additional electronic equipment and the complexity of such schemes may prohibit their use, however. In any case, the simple system proposed here should serve to demonstrate the performance of the SIXPAC in a desaturation mode.

To study this performance, both single-axis and multiple-axis desaturations are examined. For the single-axis desaturation, the inner gimbal angle α_{YX} which provides control about the Z-axis of the spacecraft was set at 63° and the corresponding outer gimbal angle α_{XY} was set at 81°. A 30° maneuver at a rate of 1° per second was then commanded about the Z-axis. The corresponding motion of the example spacecraft is illustrated in figure 15.

Figure 15(a) presents the rate and attitude of the spacecraft about the maneuver axis, and it may be seen that the final position is achieved in about 35 seconds. The maneuver is essentially unaffected by the desaturation.

Figure 15(b) gives the gimbal angles and the desaturation torque. The inner gimbal angle α_{YX} reaches its 70° stop at 0.6 second and the corresponding outer gimbal angle α_{XY} simultaneously approaches 90°. The Z-axis desaturation jet is automatically fired,

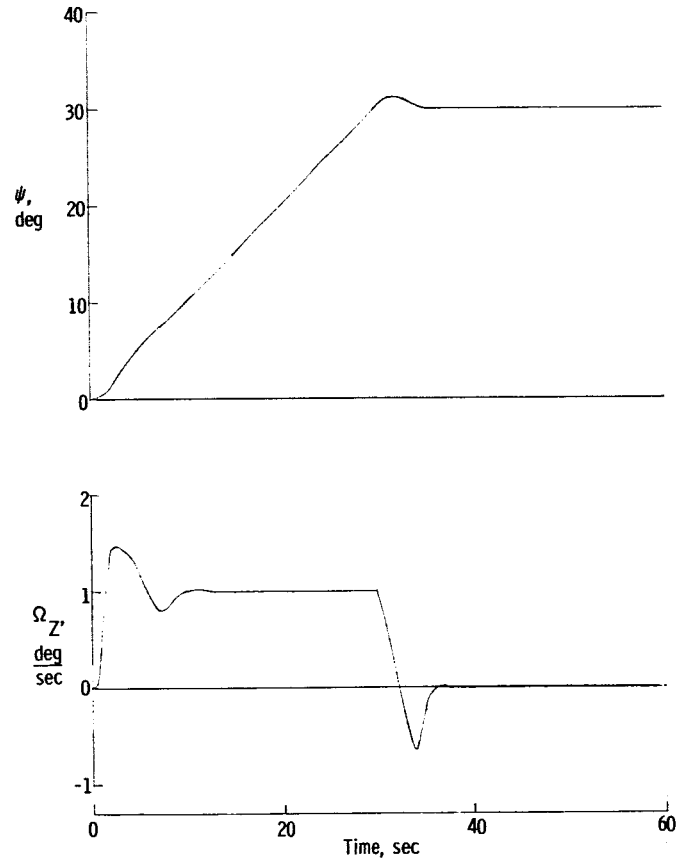

(a) Tracking angle and rate.

Figure 15.- Single-axis desaturation.

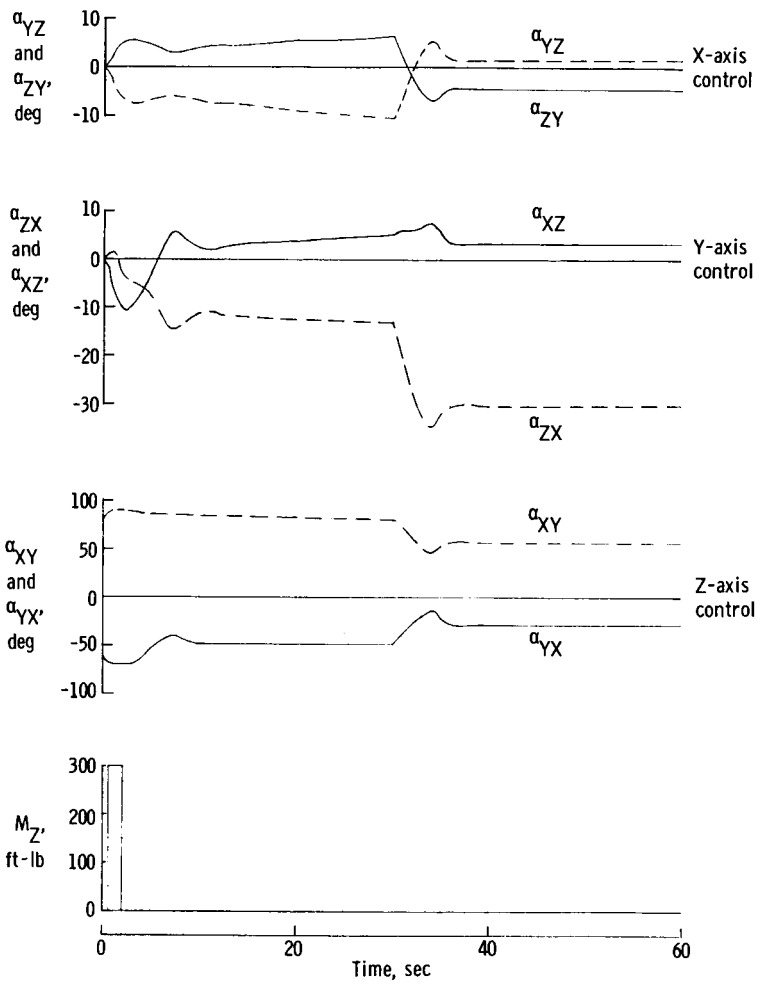

(b) Gimbal motion and desaturation torque.

Figure 15.- Concluded.

and three consecutive desaturation pulses are required to complete the desaturation. Fuel consumption during the maneuver was 0.25 pound (0.1134 kg) and average power consumption was 99 watts.

Multiple desaturations about all three axes of the spacecraft may also be required. To simulate such desaturations all inner gimbal angles were set at 63^{o} and the corresponding outer gimbal angles were set at 81^{o}. Simultaneous 30^{o} maneuvers at Euler rates of 0.5^{o} per second were commanded for the simulation, and the resultant spacecraft response is shown in figure 16.

As is apparent from figure 16(a), the spacecraft maneuvers are completed in about 60 seconds. Gimbal angles and desaturation torques, given in figure 16(b), are similar to the single-axis desaturations but exhibit considerably greater cross-coupling effects; therefore, 22 desaturation pulses with a fuel consumption of 0.625 pound (0.2835 kg) were necessary. Average consumed power for the maneuver was 119 watts.

These two examples are "worst case" types of desaturations, and will probably be required only rarely in an actual flight since the crew of the spacecraft can in general select the maneuver direction to avoid desaturation during maneuvers. Normal desaturation is expected to occur during crew motions and external torques.

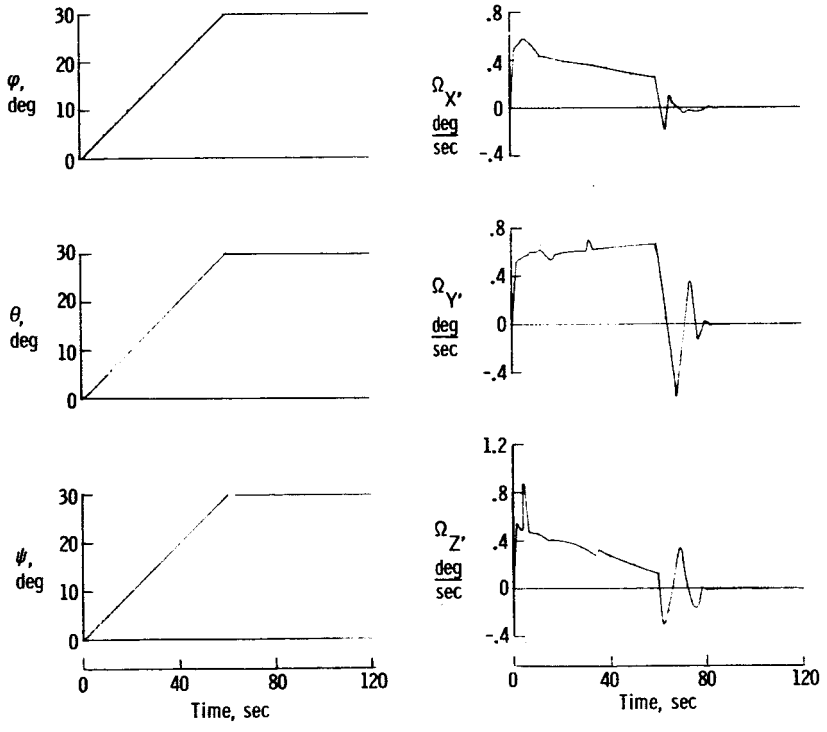

(a) Tracking angles and rates.

Figure 16.- Multiple-axis desaturation.

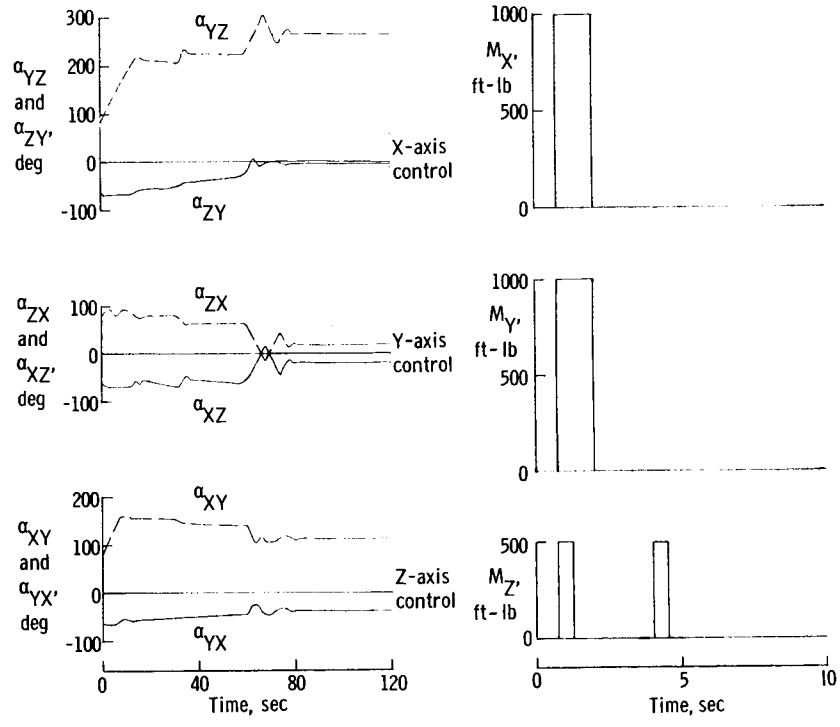

(b) Gimbal motion and desaturation torques.

Figure 16.- Concluded.

Failure modes.- An analysis of the SIXPAC should also include consideration of the system performance in the event that one of the three gyros should fail. The probability of such a failure in an actual flight will, of course, be very low. (See ref. 8.) Malfunctioning of a gyro component may, however, require shutdown of one of the gyros during repair.

To simulate such a failure on the computer, the X-axis gyro contribution was removed from the control-system equations. A typical crew motion (fig. 7(a)) was then assumed to occur, and the controlled spacecraft response with this crew motion is illustrated in figure 17. This figure should be compared with figures 7(c) and 7(d) where the complete SIXPAC provided control.

From figure 17(a), one notes that the attitude errors are now held to less than 0.3^{o}, as compared with 0.17^{o} for the entire SIXPAC (fig. 7(c)). After completion of the motion, the errors are again damped to zero. This damping is somewhat slower than that of figure 7(c), since the SIXPAC control gains were not selected for the two gyro control modes. Gimbal motions (fig. 17(b)) are correspondingly greater than those in figure 7(d), and the average power consumption was 90 watts.

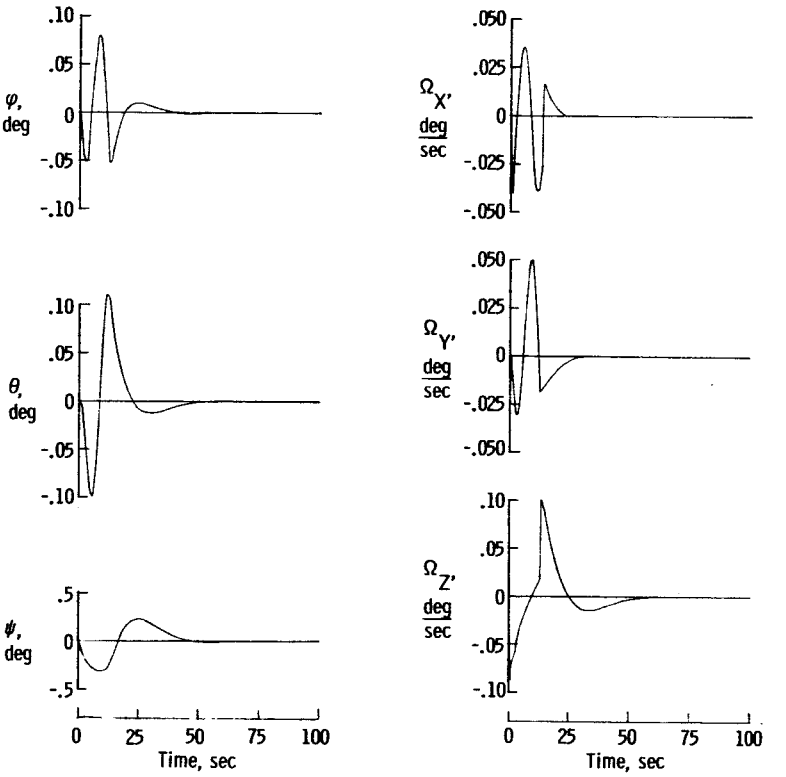

(a) Spacecraft motion.

Figure 17.- Failure-mode operation.

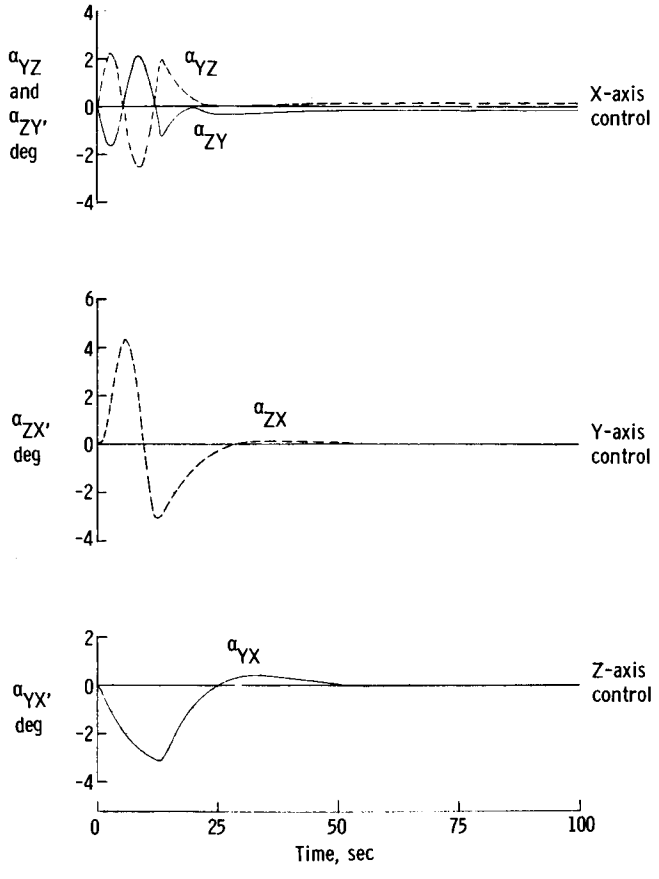

(b) Gimbal motion.

Figure 17.- Concluded.

A number of similar simulations considering failure of single gyros for different spacecraft axes have shown that the SIXPAC can provide reduced control in case of failure of any single gyro. Changes in the control gains to incorporate such a failure mode further improved the failure-mode response, but may add considerably to the SIXPAC complexity. Maneuver and experiment tasks should be minimized during the failure modes.

It appears advisable to incorporate the desaturation jets in a backup control loop that can be used for control of the spacecraft in emergency modes. No attempt to generate such a control loop was made here.

CONCLUDING REMARKS

A computer analysis of a system for experiment pointing and attitude control (designated SIXPAC) has shown that this control system can accomplish both coarse and fine attitude control for future manned spacecraft. Maximum maneuver rates of about 1.0^{o} per second and pointing axis accuracies of 0.1 arc second were achieved for an example Apollo applications mission. The SIXPAC weight should be considerably less than that for equivalent reaction-jet, reaction-wheel, or control moment gyro systems for long-term missions, and the average power consumption for the Apollo application was less than 110 watts.

Desaturation and failure modes for the SIXPAC were also examined. A simple desaturation scheme using pulsed reaction jets proved to be acceptable and could be used as a backup control system in case of complete failure of the SIXPAC gyros. For failure of any one of the three SIXPAC gyros, satisfactory coarse control was provided by the remaining two gyros.

The development of the control moment gyros required for SIXPAC represents a significant advance in the present state of the art of control components. An experimental program will thus be necessary to substantiate the performance characteristics of the SIXPAC with its idealized gyro simulations.

Langley Research Center,
National Aeronautics and Space Administration,
Langley Station, Hampton, Va., March 29, 1966.

APPENDIX A

SPACECRAFT EQUATIONS OF MOTION

The motion of the spacecraft is defined with respect to the reference system shown in figure 2. A set of XYZ axes fixed to the spacecraft here determines the angular motion of the spacecraft relative to a set of intermediate X_I, Y_I, and Z_I axes. The intermediate axes translate without rotation in inertial space, but always remain parallel to a set of X_F, Y_F, and Z_F axes fixed in inertial space.

The inertial attitude of the spacecraft is specified by three modified Euler angles, which determine the relative motion between the X, Y, and Z and the X_I, Y_I, and Z_I axes. These modified Euler angles, illustrated in figure 3, result from three consecutive rotations. The first rotation, about the Z_I axis, takes the X_I and Y_I axes through an angle ψ measured in a horizontal plane. The second rotation, about the Y_I' axis, then carries the X_I' and Z_I' axes through an angle θ measured in a vertical plane. Finally, the third rotation, about the X_I'' axis, carries the Y_I'' and Z_I'' axes through the angle φ measured in an inclined plane to give the X, Y, and Z axes.

The modified Euler angles are determined by expressing the time derivatives $\dot{\psi}$, $\dot{\theta}$, and $\dot{\varphi}$ in terms of the angular rates Ω_X, Ω_Y, and Ω_Z about the axes of the spacecraft. These angular rates then can be found from a solution of the vehicle force and moment equations. The resulting relations for Ω_X, Ω_Y, and Ω_Z are substituted into the Euler transformations, which now reduce to differential equations in ψ, θ, φ, and time t. The solutions of these equations give the attitude variation of the spacecraft relative to the intermediate axes and thus determine the angular motion of the spacecraft.

From figure 3, the time derivatives of the Euler angles become

$$\left.\begin{aligned} \dot{\varphi} &= \Omega_X + \Omega_Y \tan\theta \sin\varphi + \Omega_Z \tan\theta \cos\varphi \\ \dot{\theta} &= \Omega_Y \cos\varphi - \Omega_Z \sin\varphi \\ \dot{\psi} &= \Omega_Z \cos\varphi \sec\theta + \Omega_Y \sin\varphi \sec\theta \end{aligned}\right\} \tag{A1}$$

To allow the determination of the body rates in equations (A1), the spacecraft is taken as a large mass m_S fixed with respect to the X, Y, and Z axes and n smaller masses representing crew members or cargo and moving relative to the X, Y, and Z axes. If the position coordinates of the jth moving mass m_j are x_j, y_j, and z_j, the equations of motion are

APPENDIX A

$$
\begin{aligned}
M_X + G_X = {} & y_S F_Z - z_S F_Y + I_X\dot{\Omega}_X - I_{XY}\dot{\Omega}_Y - I_{XZ}\dot{\Omega}_Z + \dot{I}_X\Omega_X - \dot{I}_{XY}\Omega_Y - \dot{I}_{XZ}\Omega_Z \\
& - \Omega_Z\left(I_Y\Omega_Y - I_{YZ}\Omega_Z - I_{YX}\Omega_X\right) + \Omega_Y\left(I_Z\Omega_Z - I_{ZX}\Omega_X - I_{ZY}\Omega_Y\right) \\
& + \left[\sum_{j=1}^{n} m_j\left(x_j\dot{y}_j - y_j\dot{x}_j\right) - m_S\left(x_S\dot{y}_S - y_S\dot{x}_S\right)\right]\Omega_Y \\
& + \left[\sum_{j=1}^{n} m_j\left(x_j\dot{z}_j - z_j\dot{x}_j\right) - m_S\left(x_S\dot{z}_S - z_S\dot{x}_S\right)\right]\Omega_Z \\
& + \left[\sum_{j=1}^{n} m_j\left(y_j\ddot{z}_j - z_j\ddot{y}_j\right) - m_S\left(y_S\ddot{z}_S - z_S\ddot{y}_S\right)\right]
\end{aligned} \tag{A2}
$$

$$
\begin{aligned}
M_Y + G_Y = {} & z_S F_X - x_S F_Z + I_Y\dot{\Omega}_Y - I_{YZ}\dot{\Omega}_Z - I_{YX}\dot{\Omega}_X + \dot{I}_Y\Omega_Y - \dot{I}_{YZ}\Omega_Z - \dot{I}_{YX}\Omega_X \\
& - \Omega_X\left(I_Z\Omega_Z - I_{ZX}\Omega_X - I_{ZY}\Omega_Y\right) + \Omega_Z\left(I_X\Omega_X - I_{XY}\Omega_Y - I_{XZ}\Omega_Z\right) \\
& + \left[\sum_{j=1}^{n} m_j\left(y_j\dot{x}_j - x_j\dot{y}_j\right) - m_S\left(y_S\dot{x}_S - x_S\dot{y}_S\right)\right]\Omega_X \\
& + \left[\sum_{j=1}^{n} m_j\left(y_j\dot{z}_j - z_j\dot{y}_j\right) - m_S\left(y_S\dot{z}_S - z_S\dot{y}_S\right)\right]\Omega_Z \\
& + \left[\sum_{j=1}^{n} m_j\left(z_j\ddot{x}_j - x_j\ddot{z}_j\right) - m_S\left(z_S\ddot{x}_S - x_S\ddot{z}_S\right)\right]
\end{aligned} \tag{A3}
$$

and

$$
\begin{aligned}
M_Z + G_Z = {} & x_S F_Y - y_S F_X + I_Z\dot{\Omega}_Z - I_{ZX}\dot{\Omega}_X - I_{ZY}\dot{\Omega}_Y + \dot{I}_Z\Omega_Z - \dot{I}_{ZX}\Omega_X - \dot{I}_{ZY}\Omega_Y \\
& - \Omega_Y\left(I_X\Omega_X - I_{XY}\Omega_Y - I_{XZ}\Omega_Z\right) + \Omega_X\left(I_Y\Omega_Y - I_{YZ}\Omega_Z - I_{YX}\Omega_X\right) \\
& + \left[\sum_{j=1}^{n} m_j\left(z_j\dot{x}_j - x_j\dot{z}_j\right) - m_S\left(z_S\dot{x}_S - x_S\dot{z}_S\right)\right]\Omega_X \\
& + \left[\sum_{j=1}^{n} m_j\left(z_j\dot{y}_j - y_j\dot{z}_j\right) - m_S\left(z_S\dot{y}_S - y_S\dot{z}_S\right)\right]\Omega_Y \\
& + \left[\sum_{j=1}^{n} m_j\left(x_j\ddot{y}_j - y_j\ddot{x}_j\right) - m_S\left(x_S\ddot{y}_S - y_S\ddot{x}_S\right)\right]
\end{aligned} \tag{A4}
$$

These equations follow directly from expansion of the vector relations for the general motion of spinning bodies with varying configuration. (See ref. 10.)

The inertia terms in these equations are

$$\left.\begin{aligned}
I_X &= I_{XS} + \sum_{j=1}^{n} m_j\left(y_j^2 + z_j^2\right) - m_S\left(y_s^2 + z_s^2\right) \\
I_Y &= I_{YS} + \sum_{j=1}^{n} m_j\left(x_j^2 + z_j^2\right) - m_S\left(x_s^2 + z_s^2\right) \\
I_Z &= I_{ZS} + \sum_{j=1}^{n} m_j\left(x_j^2 + y_j^2\right) - m_S\left(x_s^2 + y_s^2\right) \\
I_{XZ} &= \sum_{j=1}^{n} m_j\left(x_j z_j\right) - m_S\left(x_s z_s\right) \\
I_{YZ} &= \sum_{j=1}^{n} m_j\left(y_j z_j\right) - m_S\left(y_s z_s\right) \\
I_{XY} &= \sum_{j=1}^{n} m_j\left(x_j y_j\right) - m_S\left(x_s y_s\right)
\end{aligned}\right\} \qquad \text{(A5)}$$

and

$$\left.\begin{aligned}
\dot{I}_X &= 2\left[\sum_{j=1}^{n} m_j\left(y_j\dot{y}_j + z_j\dot{z}_j\right) - m_S\left(y_s\dot{y}_s + z_s\dot{z}_s\right)\right] \\
\dot{I}_Y &= 2\left[\sum_{j=1}^{n} m_j\left(x_j\dot{x}_j + z_j\dot{z}_j\right) - m_S\left(x_s\dot{x}_s + z_s\dot{z}_s\right)\right] \\
\dot{I}_Z &= 2\left[\sum_{j=1}^{n} m_j\left(x_j\dot{x}_j + y_j\dot{y}_j\right) - m_S\left(x_s\dot{x}_s + y_s\dot{y}_s\right)\right] \\
\dot{I}_{XZ} &= \sum_{j=1}^{n} m_j\left(x_j\dot{z}_j + z_j\dot{x}_j\right) - m_S\left(x_s\dot{z}_s + z_s\dot{x}_s\right) \\
\dot{I}_{YZ} &= \sum_{j=1}^{n} m_j\left(y_j\dot{z}_j + z_j\dot{y}_j\right) - m_S\left(y_s\dot{z}_s + z_s\dot{y}_s\right) \\
\dot{I}_{XY} &= \sum_{j=1}^{n} m_j\left(x_j\dot{y}_j + y_j\dot{x}_j\right) - m_S\left(x_s\dot{y}_s + y_s\dot{x}_s\right)
\end{aligned}\right\} \qquad \text{(A6)}$$

APPENDIX A

The coordinates x_S, y_S, and z_S of the composite mass center become

$$\left.\begin{aligned} x_S &= \sum_{j=1}^{n} \frac{m_j}{m_S} x_j \\ y_S &= \sum_{j=1}^{n} \frac{m_j}{m_S} y_j \\ z_S &= \sum_{j=1}^{n} \frac{m_j}{m_S} z_j \end{aligned}\right\} \tag{A7}$$

with respect to the X, Y, and Z axes.

Disturbance torques are represented by the moments M_X, M_Y, and M_Z and the moments due to noncoincidence of the composite mass center and the origin of the X, Y, and Z system. Translation of the mass center caused by the forces F_X, F_Y, and F_Z thus requires the inclusion of these terms in the equations of motion.

For the present analysis it is assumed that all disturbance torques result from pure couples with

$$F_X = F_Y = F_Z = 0 \tag{A8}$$

and that the disturbance torques can be approximated by

$$\left.\begin{aligned} M_X &= M_{X1} + M_{X2} \cos\left(M_{X3}t + M_{X4}\right) + M_{X5} \cos\left(M_{X6}t + M_{X7}\right) + \Delta M_X \\ M_Y &= M_{Y1} + M_{Y2} \cos\left(M_{Y3}t + M_{Y4}\right) + M_{Y5} \cos\left(M_{Y6}t + M_{Y7}\right) + \Delta M_Y \\ M_Z &= M_{Z1} + M_{Z2} \cos\left(M_{Z3}t + M_{Z4}\right) + M_{Z5} \cos\left(M_{Z6}t + M_{Z7}\right) + \Delta M_Z \end{aligned}\right\} \tag{A9}$$

These moments are used to simulate gravity-gradient, aerodynamic, and desaturation torques that act on the spacecraft.

The definition of the control torques G_X, G_Y, and G_Z completes the development of the equations of motion. These torques are derived in appendix B.

Solution of equations (A2) to (A4), after substitution for all applicable torques and mass-motion terms, now yields the body rates Ω_X, Ω_Y, and Ω_Z. The Euler angles follow from equations (A1) and the angular motion of the spacecraft has thus been defined.

APPENDIX B

CONTROL SYSTEM EQUATIONS

Spacecraft Control Torques

The control torques for the SIXPAC are developed by commanding changes in the angular momentum components of the SIXPAC gyros along the body axes. Each of these gyros is mounted on double gimbals, and the necessary momentum components along a spacecraft axis are implemented by controlling the position of these gimbals with respect to the spacecraft axes. The reaction torque applied to the spacecraft by the resultant precession of the gyro momenta is

$$\overline{G} = -\left[\dot{\overline{H}} + (\overline{\Omega} \times \overline{H})\right] \tag{B1}$$

where $\overline{\Omega}$ is the total angular velocity vector of the spacecraft, and $\overline{H}$ is the total angular momentum vector of the SIXPAC. The definition of these vectors requires the determination of the gyro momenta and gimbal torque components along the body axes in terms of the gimbal angles.

To simplify manipulations with these components, the following representation is introduced. The gimbal angles and the gimbal rate and torque components are defined by α_{pq} or α_{qp}, $\dot{\alpha}_{pq}$ or $\dot{\alpha}_{qp}$, and T_{pq} or T_{qp}, respectively. The subscripts p and q can be either X, Y, or Z, with $p \neq q$. The first subscript refers to the reference axis of the gyro under consideration and the second subscript refers to the axis with which the component or angle is associated. This latter axis is a spacecraft axis for even permutations (ZX, XY, YZ) of the subscripts and is an intermediate gimbal axis for odd permutations (XZ, ZY, YX) of the subscripts. Even permutation in the subscripts is indicated by the symbol α_{pq} and odd permutation by the symbol α_{qp}.

The corresponding gyro momenta, the spacecraft and gimbal rates, and the gimbal torques are depicted in figure 18. From the figure, it follows that

$$\left.\begin{aligned} \overline{G} \equiv \begin{pmatrix} G_X \\ G_Y \\ G_Z \end{pmatrix} &= -\begin{pmatrix} T_{ZX} + T_{YX}\cos\alpha_{YZ} + T_{XZ}\sin\alpha_{XY} \\ T_{XY} + T_{ZY}\cos\alpha_{ZX} + T_{YX}\sin\alpha_{YZ} \\ T_{YZ} + T_{XZ}\cos\alpha_{XY} + T_{ZY}\sin\alpha_{ZX} \end{pmatrix} \\ \overline{\Omega} &= \begin{pmatrix} \Omega_X \\ \Omega_Y \\ \Omega_Z \end{pmatrix} \end{aligned}\right\} \tag{B2}$$

APPENDIX B

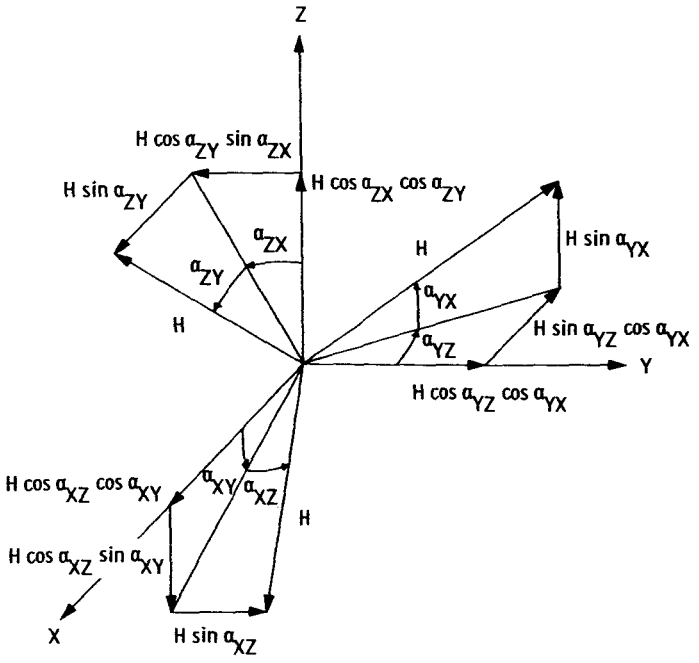

(a) Gyro momentum components.

Figure 18.- Vector representations of SIXPAC momentum, angular velocity, and gimbal torque components.

and

$$\overline{H} = H\begin{pmatrix} \cos \alpha_{XZ} \cos \alpha_{XY} - \cos \alpha_{YX} \sin \alpha_{YZ} + \sin \alpha_{ZY} \\ \cos \alpha_{YX} \cos \alpha_{YZ} - \cos \alpha_{ZY} \sin \alpha_{ZX} + \sin \alpha_{XZ} \\ \cos \alpha_{ZY} \cos \alpha_{ZX} - \cos \alpha_{XZ} \sin \alpha_{XY} + \sin \alpha_{YX} \end{pmatrix} \tag{B3}$$

The control torque components G_X, G_Y, and G_Z are now given by substitution of equations (B2) and (B3) into equation (B1).

Thus, after some simplification,

$$\left.\begin{aligned} G_X &= -\left(T_{ZX} + T_{YX} \cos \alpha_{YZ} + T_{XZ} \sin \alpha_{XY}\right) \\ G_X &= H\Big[\left(\Omega_Z + \dot{\alpha}_{YZ}\right)\cos \alpha_{YX} \cos \alpha_{YZ} + \left(\Omega_Y + \dot{\alpha}_{XY}\right)\cos \alpha_{XZ} \sin \alpha_{XY} \\ &\quad - \left(\Omega_Y + \dot{\alpha}_{YX} \sin \alpha_{YZ}\right)\sin \alpha_{YX} + \left(\Omega_Z + \dot{\alpha}_{XZ} \cos \alpha_{XY}\right)\sin \alpha_{XZ} \\ &\quad - \left(\Omega_Z \sin \alpha_{ZX} + \Omega_Y \cos \alpha_{ZX} + \dot{\alpha}_{ZY}\right)\cos \alpha_{ZY}\Big] \end{aligned}\right\} \tag{B4}$$

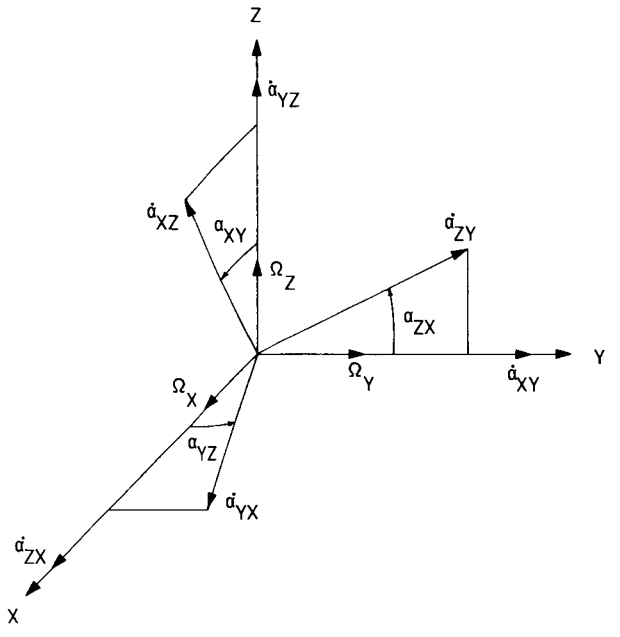

(b) Angular velocity components.

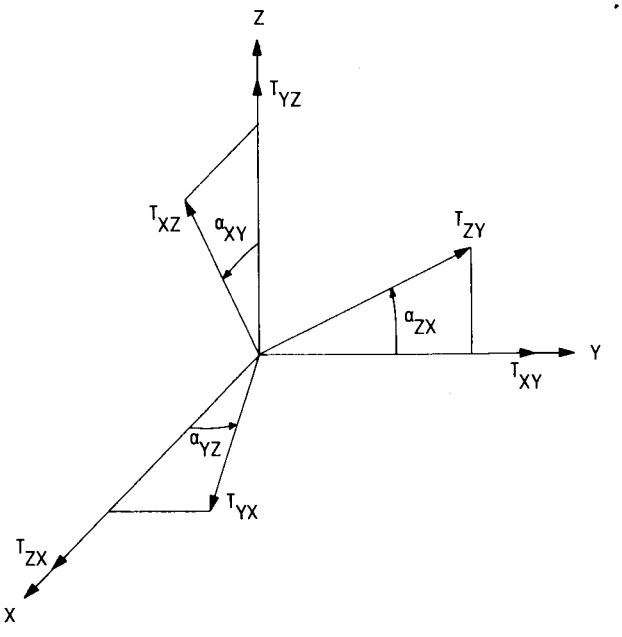

(c) Gimbal torque components.

Figure 18.- Concluded.

$$\left.\begin{aligned} G_Y &= -\left(T_{XY} + T_{ZY}\cos\alpha_{ZX} + T_{YX}\sin\alpha_{YZ}\right) \\ G_Y &= H\Big[\left(\Omega_X + \dot{\alpha}_{ZX}\right)\cos\alpha_{ZY}\cos\alpha_{ZX} + \left(\Omega_Z + \dot{\alpha}_{YZ}\right)\cos\alpha_{YX}\sin\alpha_{YZ} \\ &\quad - \left(\Omega_Z + \dot{\alpha}_{ZY}\sin\alpha_{ZX}\right)\sin\alpha_{ZY} + \left(\Omega_X + \dot{\alpha}_{YX}\cos\alpha_{YZ}\right)\sin\alpha_{YX} \\ &\quad - \left(\Omega_X\sin\alpha_{XY} + \Omega_Z\cos\alpha_{XY} + \dot{\alpha}_{XZ}\right)\cos\alpha_{XZ}\Big] \end{aligned}\right\} \quad \text{(B5)}$$

and

$$\left.\begin{aligned} G_Z &= -\left(T_{YZ} + T_{XZ}\cos\alpha_{XY} + T_{ZY}\sin\alpha_{ZX}\right) \\ G_Z &= H\Big[\left(\Omega_Y + \dot{\alpha}_{XY}\right)\cos\alpha_{XZ}\cos\alpha_{XY} + \left(\Omega_X + \dot{\alpha}_{ZX}\right)\cos\alpha_{ZY}\sin\alpha_{ZX} \\ &\quad - \left(\Omega_X + \dot{\alpha}_{XZ}\sin\alpha_{XY}\right)\sin\alpha_{XZ} + \left(\Omega_Y + \dot{\alpha}_{ZY}\cos\alpha_{ZX}\right)\sin\alpha_{ZY} \\ &\quad - \left(\Omega_Y\sin\alpha_{YZ} + \Omega_X\cos\alpha_{YZ} + \dot{\alpha}_{YX}\right)\cos\alpha_{YX}\Big] \end{aligned}\right\} \quad \text{(B6)}$$

Equations (B4) to (B6) are the control torque components applied to the spacecraft by the SIXPAC gimbal motions. The computation of these torques necessitates the definition of the gimbal angles and rates.

Gimbal Angles and Rates

The gimbal rates are commanded to be proportional to the spacecraft rates and attitude, since this form of command is both stable and easy to mechanize. To develop the necessary gimbal angle relations, one may introduce the functions

$$\left.\begin{aligned} k_1 &= -K_1(\psi - \psi_c) - K_2(\Omega_Z - \Omega_{Zc}) \\ k_2 &= -K_3(\theta - \theta_c) - K_4(\Omega_Y - \Omega_{Yc}) \\ k_3 &= -K_5(\varphi - \varphi_c) - K_6(\Omega_X - \Omega_{Xc}) \\ k_4 &= K_7(\psi - \psi_c) + K_8(\Omega_Z - \Omega_{Zc}) \\ k_5 &= K_9(\theta - \theta_c) + K_{10}(\Omega_Y - \Omega_{Yc}) \\ k_6 &= K_{11}(\varphi - \varphi_c) + K_{12}(\Omega_X - \Omega_{Xc}) \end{aligned}\right\} \tag{B7}$$

where ψ, θ, φ, Ω_X, Ω_Y, and Ω_Z are determined by sensors onboard the spacecraft and in this analysis are found by integration of the equations of motion. The terms Ω_{Xc}, Ω_{Yc}, Ω_{Zc}, φ_c, θ_c, and ψ_c are used to allow for command of spacecraft rates that may be required for maneuvers and slewing missions. The desired spacecraft rates are taken as

$$\left.\begin{aligned} \Omega_{Xc} &= \dot{\varphi}_m - \dot{\psi}_m \sin \dot{\theta}_m t + \Omega_{Xe} \\ \Omega_{Yc} &= \dot{\theta}_m \cos \dot{\varphi}_m t + \dot{\psi}_m \sin \dot{\varphi}_m t \cos \dot{\theta}_m t + \Omega_{Ye} \\ \Omega_{Zc} &= \dot{\psi}_m \cos \dot{\varphi}_m t \cos \dot{\theta}_m t - \dot{\theta}_m \sin \dot{\varphi}_m t + \Omega_{Ze} \end{aligned}\right\} \tag{B8}$$

where the magnitudes and on times of $\dot{\varphi}_m$, $\dot{\theta}_m$, and $\dot{\psi}_m$ are set for a particular maneuver, and the terms Ω_{Xe}, Ω_{Ye}, and Ω_{Ze} are the spacecraft rates required for the experiment control tasks.

The Euler angles associated with the commanded body rates are found by integration of the relations

$$\left.\begin{aligned}
\dot{\varphi}_c &= \Omega_{Xc} + \Omega_{Yc} \tan \theta_c \sin \varphi_c + \Omega_{Zc} \tan \theta_c \cos \varphi_c \\
\dot{\theta}_c &= \Omega_{Yc} \cos \varphi_c - \Omega_{Zc} \sin \varphi_c \\
\dot{\psi}_c &= \Omega_{Zc} \cos \varphi_c \sec \theta_c + \Omega_{Yc} \sin \varphi_c \sec \theta_c
\end{aligned}\right\} \tag{B9}$$

By selecting values for $\dot{\varphi}_m$, $\dot{\theta}_m$, and $\dot{\psi}_m$, various maneuver rates can be commanded for the spacecraft.

To apply the necessary control torques, the gimbal angles are rate-stabilized by using the relations:

$$\left.\begin{aligned}
\dot{\alpha}_{XY} &= k_1 \cos \alpha_{XY} + k_3 \sin \alpha_{XY} \\
\dot{\alpha}_{ZX} &= k_2 \cos \alpha_{ZX} + k_1 \sin \alpha_{ZX} \\
\dot{\alpha}_{YZ} &= k_3 \cos \alpha_{YZ} + k_2 \sin \alpha_{YZ} \\
\dot{\alpha}_{YX} &= k_4 \cos \alpha_{YX} \\
\dot{\alpha}_{XZ} &= k_5 \cos \alpha_{XZ} \\
\dot{\alpha}_{ZY} &= k_6 \cos \alpha_{ZY}
\end{aligned}\right\} \tag{B10}$$

where the gimbal angles are measured in the actual spacecraft flight and are determined by numerical integration of equations (B10). This control law allows full use of the angular momentum capacity for each gyro by weighting the gimbal rate in terms of the resultant gimbal angle. Substitution of the gimbal rates and the gimbal angles derived from equations (B10) into equations (B4) to (B6) now allows the computations of the control torque components for the SIXPAC concept for particular control gains.

Control Gain Development

Approximate values of the control gains may be determined by linearizing the equations of motion for very small gimbal angles, small body rates, and small Euler angles. One thus has

$$\sin \alpha_{pq} \to 0$$

$$\sin \alpha_{qp} \to 0$$

$$\cos \alpha_{pq} \to 1$$

$$\cos \alpha_{qp} \to 1$$

and

$$\left.\begin{aligned} G_X &\approx H\left(\dot{\alpha}_{YZ} - \dot{\alpha}_{ZY}\right) \\ G_Y &\approx H\left(\dot{\alpha}_{ZX} - \dot{\alpha}_{XZ}\right) \\ G_Z &\approx H\left(\dot{\alpha}_{XY} - \dot{\alpha}_{YX}\right) \end{aligned}\right\} \tag{B11}$$

Substitution for the gimbal rates gives

$$\left.\begin{aligned} G_X &\approx -H\left[\left(K_5 + K_{11}\right)\left(\varphi - \varphi_c\right) + \left(K_6 + K_{12}\right)\left(\Omega_X - \Omega_{Xc}\right)\right] \\ G_Y &\approx -H\left[\left(K_3 + K_9\right)\left(\theta - \theta_c\right) + \left(K_4 + K_{10}\right)\left(\Omega_Y - \Omega_{Yc}\right)\right] \\ G_Z &\approx -H\left[\left(K_1 + K_7\right)\left(\psi - \psi_c\right) + \left(K_2 + K_8\right)\left(\Omega_Z - \Omega_{Zc}\right)\right] \end{aligned}\right\} \tag{B12}$$

The assumption that the body rates and Euler angles are small also yields

$$\left.\begin{aligned} \varphi - \varphi_c &\approx \int \left(\Omega_X - \Omega_{Xc}\right)dt \\ \theta - \theta_c &\approx \int \left(\Omega_Y - \Omega_{Yc}\right)dt \\ \psi - \psi_c &\approx \int \left(\Omega_Z - \Omega_{Zc}\right)dt \end{aligned}\right\} \tag{B13}$$

and

$$\left.\begin{aligned} G_X &\approx I_X\dot{\Omega}_X - M_X + f_X\left(x_j, y_j, z_j\right) \\ G_Y &\approx I_Y\dot{\Omega}_Y - M_Y + f_Y\left(x_j, y_j, z_j\right) \\ G_Z &\approx I_Z\dot{\Omega}_Z - M_Z + f_Z\left(x_j, y_j, z_j\right) \end{aligned}\right\} \tag{B14}$$

where $f\left(x_j, y_j, z_j\right)$ represents the torques caused by mass motion within the spacecraft. Combination of equations (B14) and (B12) now results in equations of the form

$$\dot{\Omega} - \dot{\Omega}_c + \left(\frac{HK_r}{I}\right)\left(\Omega - \Omega_c\right) + \left(\frac{HK_a}{I}\right)\int \left(\Omega - \Omega_c\right)dt = \frac{1}{I}(M + f) - \dot{\Omega}_c \tag{B15}$$

for each axis. The gains K_r and K_a are the sum of the inner and outer gimbal gains

$$\left.\begin{aligned} K_r &= K_{r_i} + K_{r_o} \\ K_a &= K_{a_i} + K_{a_o} \end{aligned}\right\} \tag{B16}$$

and the characteristic equation becomes

$$s^2 + \frac{HK_r}{I} s + \frac{HK_a}{I} = 0 \tag{B17}$$

This equation has the form

$$s^2 + 2\rho\omega_n s + \omega_n^2 = 0 \tag{B18}$$

with the response parameters

$$\left.\begin{aligned} &\text{Natural frequency} \equiv \omega_n = \sqrt{\frac{HK_a}{I}} \\ &\text{Damping ratio} \equiv \rho = \frac{K_r}{2}\sqrt{\frac{H}{IK_a}} \\ &\text{Time constant} \equiv \tau \equiv \frac{1}{\rho\omega_n} = \frac{2I}{HK_r} \end{aligned}\right\} \tag{B19}$$

From equations (B19), the control gains may be written as

$$K_r = \frac{2I}{H\tau} \tag{B20}$$

and

$$K_a = \frac{I}{H\rho^2\tau^2} \tag{B21}$$

The inner and outer gimbals should reach their effective limits at the same time; hence, one selects

$$K_i = \left(\frac{\alpha_{qpL}}{90}\right) K_o \equiv LK_o \tag{B22}$$

where qp denotes the odd permutation. Values of the gains may now be computed from

$$\left.\begin{aligned} K_{r_o} &= \frac{2}{1+L}\frac{I}{H\tau} \\ K_{r_i} &= \frac{2L}{1+L}\frac{I}{H\tau} \end{aligned}\right\} \tag{B23}$$

and

$$\left.\begin{aligned} K_{a_o} &= \frac{1}{1+L}\frac{I}{H\rho^2\tau^2} \\ K_{a_i} &= \frac{L}{1+L}\frac{I}{H\rho^2\tau^2} \end{aligned}\right\} \tag{B24}$$

for desired values of damping ratio and time constant. The resulting gains should then lead to stable response of the spacecraft, but their effectiveness must, of course, be verified in the nonlinear region.

Gimbal Mechanization and Desaturation

Gimbal motions for the SIXPAC must be bounded to avoid the possibility of gimbal lock. The outer gimbals cannot incur gimbal lock and thus are capable of continuous rotation. The inner gimbals, however, move into gimbal lock at $\pm 90^o$ and the absolute value of the inner gimbal angles must be restricted to be less than or equal to a limiting value α_{qpL}, which in turn is smaller than 90^o.

The angle α_{qpL} is then the angle at which a condition of maximum momentum storage is reached for the inner gimbal. From an examination of the control gains selected for the SIXPAC gimbals, it is apparent that the corresponding outer gimbal angle α_{pqL} will simultaneously tend towards its maximum momentum storage position of 90^o. Control about the associated $(p \times q)$ spacecraft axis is still possible by means of the third gyro, which was originally alined with the control axis. However, the latter gyro is not always in a position where it can be effectively used for control, and a desaturation scheme must thus be provided for the SIXPAC. If the three gyros for the SIXPAC were originally selected to compensate for all anticipated cyclic torques acting on the spacecraft, this desaturation scheme will be needed primarily to counteract biased disturbance torques.

There is, of course, one exception. Saturation of the SIXPAC can also occur when all the gyro momentum vectors are colinear while control torques in the direction of the gyro momenta are required. If this condition should occur, large attitude and rate errors about the spacecraft axes may result. These errors must be eliminated by the desaturation scheme.

Such a scheme should be incorporated into the SIXPAC logic, and a reaction-jet system should be provided to allow generation of the necessary desaturation torques. No attempt to optimize the desaturation system is made in this analysis; instead, a relatively crude method of desaturation is introduced for use with the SIXPAC.

APPENDIX B

The computer simulation of this desaturation scheme is represented by the block diagram of figure 19. A series of computer checks, which test to see whether desaturation is essential, is initiated either by actuation of the gimbal stops or by failure of the control system to hold a minimum accuracy. This accuracy was selected as the coarse-mode attitude hold of 5^{o}; this upper limit should only be exceeded when the gyros saturate in a parallel position away from the inner gimbal stops.

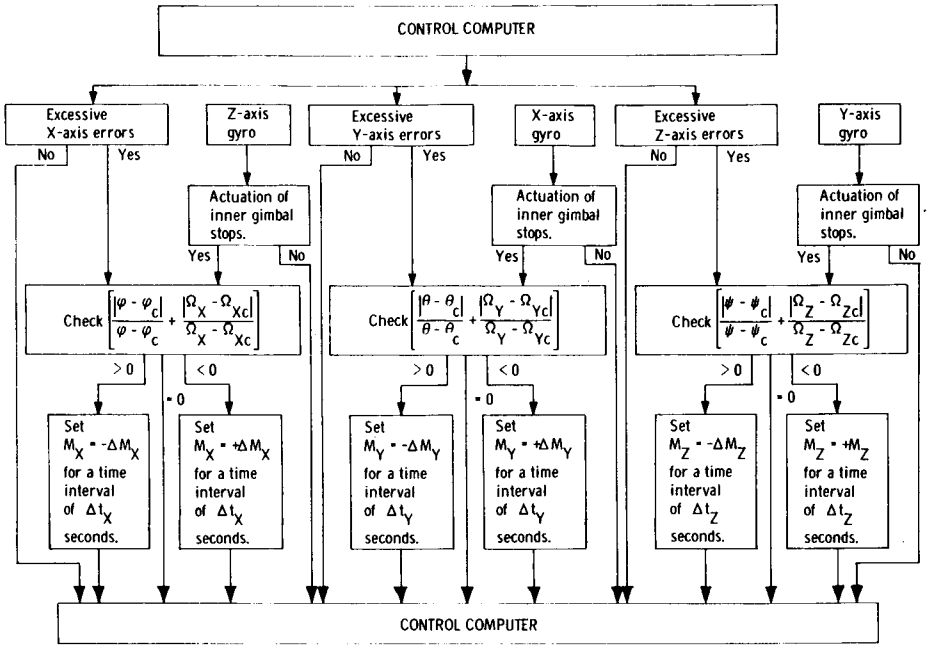

Figure 19.- Block diagram of desaturation scheme.

If a gimbal stop is reached or if the attitude limit is exceeded, the control computer examines the spacecraft sensor input to see whether control about the saturated gyro control axis is being provided by the other two SIXPAC gyros. This examination checks the sign of the rate and attitude errors for the primary control axis of the saturated gyro. If the rate and attitude errors have opposite signs, the errors will tend to zero and no desaturation is necessary. If the errors have the same signs, a positive or negative pulse moment is applied about the control axis for both signs negative or both signs positive, respectively. The amplitude and duration of the torque pulse are selected to reduce approximately the saturated gyro gimbal angle by a specified percentage, for example, 10 percent of the limiting value. The gimbals are automatically commanded to counteract the torque pulse and thus are desaturated. Such differential desaturation to about 90 percent of the limiting inner gimbal angle value assures minimum fuel consumption, since future gyro control commands may drive the inner gimbal away from its stops. Full desaturation to zero inner gimbal angle is thus unwarranted.

A more efficient version of this desaturation logic which would use only the minimum accuracy check also appears to be possible. Accuracy limits for particular experiments, maneuvers, and normal operation would now be stored on the computer and automatically used to trigger the desaturation logic. Proper selection of these limits should lead to additional fuel savings.

Power and Fuel Consumption

The gimbal torque relations may be derived from equations (B4) to (B6) with the result

$$\left.\begin{aligned}
T_{XY} &= H\Big[\left(\dot{\alpha}_{XZ} + \Omega_Z \cos \alpha_{XY} + \Omega_X \sin \alpha_{XY}\right)\cos \alpha_{XZ} + \left(\Omega_Z + \dot{\alpha}_{ZY} \sin \alpha_{ZX}\right)\sin \alpha_{ZY} \\
&\quad - \left(\Omega_X + \dot{\alpha}_{YX} \cos \alpha_{YZ}\right)\sin \alpha_{YX}\Big] \\
T_{ZX} &= H\Big[\left(\dot{\alpha}_{ZY} + \Omega_Y \cos \alpha_{ZX} + \Omega_Z \sin \alpha_{ZX}\right)\cos \alpha_{ZY} + \left(\Omega_Y + \dot{\alpha}_{YX} \sin \alpha_{YZ}\right)\sin \alpha_{YX} \\
&\quad - \left(\Omega_Z + \dot{\alpha}_{XZ} \cos \alpha_{XY}\right)\sin \alpha_{XZ}\Big] \\
T_{YZ} &= H\Big[\left(\dot{\alpha}_{YX} + \Omega_X \cos \alpha_{YZ} + \Omega_Y \sin \alpha_{YZ}\right)\cos \alpha_{YX} + \left(\Omega_X + \dot{\alpha}_{XZ} \sin \alpha_{XY}\right)\sin \alpha_{XZ} \\
&\quad - \left(\Omega_Y + \dot{\alpha}_{ZY} \cos \alpha_{ZX}\right)\sin \alpha_{ZY}\Big]
\end{aligned}\right\} \quad \text{(B25)}$$

and

$$T_{YX} = -H\left(\dot{\alpha}_{YZ} + \Omega_Z\right)\cos \alpha_{YX}$$

$$T_{XZ} = -H\left(\dot{\alpha}_{XY} + \Omega_Y\right)\cos \alpha_{XZ}$$

$$T_{ZY} = -H\left(\dot{\alpha}_{ZX} + \Omega_X\right)\cos \alpha_{ZY}$$

The theoretical output power of the gimbal torquers is thus

$$\begin{aligned}
P = 1.356\Big[&\left|T_{XY}\left(\Omega_X + \dot{\alpha}_{XY}\right)\right| + \left|T_{YZ}\left(\Omega_Z + \dot{\alpha}_{YZ}\right)\right| + \left|T_{ZX}\left(\Omega_X + \dot{\alpha}_{ZX}\right)\right| \\
&+ \left|T_{ZY}\left(\dot{\alpha}_{ZY} + \Omega_Y \cos \alpha_{ZX} + \Omega_Z \sin \alpha_{ZX}\right)\right| + \left|T_{XZ}\left(\dot{\alpha}_{XZ} + \Omega_Z \cos \alpha_{XY} + \Omega_X \sin \alpha_{XY}\right)\right| \\
&+ \left|T_{YX}\left(\dot{\alpha}_{YX} + \Omega_X \cos \alpha_{YZ} + \Omega_Y \sin \alpha_{YZ}\right)\right|\Big]
\end{aligned} \quad \text{(B26)}$$

Assumption of a gimbal torquer efficiency of 75 percent and a spin power requirement of 30 watts per gyro yields the total SIXPAC input power as

$$P_t = 90 + \frac{4P}{3} \tag{B27}$$

From equation (B27), the average power consumption becomes

$$P_{av} = 90 + \frac{4}{3\Delta t} \int^{\Delta t} P \, dt \tag{B28}$$

where Δt is the time period of interest.

Corresponding reaction-jet fuel requirements are developed from the desaturation scheme. The total fuel consumption associated with the SIXPAC operation is

$$W = \frac{1}{I_{sp}} \sum_{p=x,y,z} \int^{\Delta t} \left| \frac{\Delta M_p}{l_p} \right| dt \tag{B29}$$

where I_{sp} is the specific impulse of the reaction jets, ΔM_p are the desaturation moments, and l_p are the jet moment arms.

REFERENCES

1. Wensley, D. C.; Hayes, W. S.; and Carlisle, R. F.: Report on the Optimization of the Manned Orbital Research Laboratory (MORL) System Concept. Technical Summary Rept. SM-46086, Missile & Space Systems Div., Douglas Aircraft Co., Sept. 1964.

2. Kurzhals, Peter R.; Keckler, Claude R.; and Piland, William M.: Dynamics and Control Research Applicable to Apollo Extension Systems. Conference on Langley Research Related to Apollo Mission, 1965, pp. 303-312.

3. Kurzhals, Peter R.; Adams, James J.; and Hodge, Ward F.: Space-Station Dynamics and Control. NASA TN D-1504, 1962, pp. 71-83.

4. Kurzhals, Peter R.: Stability and Control for the Manned Orbital Laboratory. Paper presented at SAE A-18 Committee Meeting (Houston, Texas), Dec. 1963.

5. Kurzhals, Peter R.: MORL Control System Integration. Paper presented at SAE A-18 Committee Meeting (New York, N.Y.), 1964.

6. Will, Ralph W.: Performance Characteristics of Control Moment Gyro Systems for Manned Orbital Laboratories. Paper presented at SAE A-18 Committee Meeting (Miami, Fla.), 1964.

7. Yarber, G. W.; Chang, K. T.; et al.: Control Moment Gyro Optimization Study. Tech. Rept. F-8036 (Contract NAS 1-4439), Garrett Airesearch Manufacturing Div., Jan. 12, 1965.

8. Anon.: Control Moment Gyroscope Design Report. The Bendix Corp., Nov. 1, 1965.

9. Keller, J.: Description of a Disturbance Torque Computer Program. Rept. No. AB-1210-0041, Sperry Gyroscope Co., Apr. 1965.

10. Kurzhals, Peter R.: An Approximate Solution of the Equations of Motion for Arbitrary Rotating Spacecraft. Ph. D. Thesis, Virginia Polytech. Inst., 1966.